universität wien

MASTERARBEIT / MASTER'S THESIS

Titel der Masterarbeit / Title of the Master's Thesis

„Structure and dynamics of supercooled water in nanopores“

verfasst von / submitted by

Oscar Mittempergher, BSc

angestrebter akademischer Grad / in partial fulfilment of the requirements for the degree of

Master of Science (MSc)

Vienna, 2022

Studienkennzahl lt. Studienblatt / degree programme code as it appears on the student record sheet:	A 066 876
Studienrichtung lt. Studienblatt / degree programme as it appears on the student record sheet:	Masterstudium Physik
Betreut von / Supervisor:	Univ.-Prof. Dr. Christoph Dellago

Contents

Chapter 1

Abstract

Eine Substanz wird unterkühlte Flüssigkeit genannt, wenn ihre Temperatur unter dem Schmelzpunkt liegt, sie aber noch immer in der flüssigen Phase verweilt. Um das Gefrieren beim Abkühlen der Flüssigkeit unter ihrem Schmelzpunkt zu verhindern können der Flüssigkeit Substanzen beigement werden die ein Gefrieren verhindern, Kristallisationskeime aus der Flüssigkeit entfernt werden oder die Flüssigkeit in Volumina eingeschlossen werden deren Maße im Bereich einiger Nanometer liegen. In dieser Arbeit wird die Struktur und Dynamik des Wassermodells tip4p/2005, eingeschlossen in einem zylindrischen Volumen mit einem Durchmesser von 6nm, 8nm und 14nm bei verschiedenen Temperaturen und Standarddruck, mittels Molekulardynamik simuliert. Gefunden wurde Brownsche Diffusion in Richtung parallel zur Zylinderachse, und nicht-Brownsche Diffusion parallel zur Zylinderache, die auf einen nicht-verschwindenden Drehimpuls des Ensembles zurückzuführen war. Die Strukturanalyse mittels Radiusabhängiger Dichteverteilung und Paarkorrelationsfunktion deutet darauf hin, dass das Ensemble die flüssige Phase beibehielt.

Chapter 2

Introduction

When a liquid's temperature is lowered below its freezing point at constant pressure without the liquid becoming a solid it is called a supercooled liquid. A liquid state with a temperature lower than the freezing point temperature can be obtained much easier by removing any crystallisation seeds, around which a crystal structure can form, or by adding substances that inhibit freezing. An example for substances inhibiting freezing of water are some proteins produced by plants or amphibians, which they produce to survive in extremely cold environments. These proteins bind to ice crystals and prevent those ice crystals to grow and spread, an effect called freezing point depression. Another method to inhibit water freezing to ice below its freezing point temperature is to remove any crystallization seeds in the liquid. For example chemical de-mineralized water can be supercooled down to $225K$ at standard pressure.
These two described methods require to either add or remove substances solved or suspended in liquid water. An alternative method, that does not require additional substances solved or suspended in liquid water, is to confine the liquid water in volumes in the nanometre range, as shown by J. Teixeira et al. [1]. The nano-confinement of liquid water in cylindrical pores comes along with a diminished self-diffusion, depending on the pore diameter, as shown by S.T. Cui [2]. In this project we tried to analyse the behaviour of supercooled water confined in a cylindrical volume with radius r_C in the nanometre range by molecular dynamics simulation. It was inspired by the publication of [3], who measured glass transition of supercooled water in mesoporous Gelsil ($2,6nm$ and $5nm$ pore diameter) and Vycor ($10nm$ pore diameter) by means of dynamical mechanical analysis. [3] also saw a volume expansion of the probes that they assumed to result from the supercooled liquid to form a solid (glassy or crystal) core surrounded by a liquid phase. This assumption is based on the computation of the density of the liquid confined in the nano-pores and comparing it to the overall density of the examined probe. So it was clear to have a look at the radial density distribution, radius depending diffusion and radius depending structure by means of the pair correlation function. By these means it would also be possible to evaluate to what kind of structure this proposed solid core freezes, since there are several different possibilities: either a disordered glassy state or one of the different known crystal phases of water. The initial questions we tried to answer were if there is a glass transition temperature T_g and how it depends on the pore radius r_C of the pores cylindrical volume. In the following chapters the chosen model, theories and methods are explained in more detail, followed by the results and their respective interpretation and discussion.

2.1 Glass state

2.1.1 Definitions

Generally non-crystalline solids in a non-equilibrium state are called glasses. A glassy state can be obtained by solidifying a supercooled liquid or molten material. That way the internal disordered and/or randomized state of the liquid molecules/atoms positions can be preserved. So glasses

have no crystalline structure, but many of the mechanical properties are similar between crystalline and glassy states.[13][15][14]

2.2 Water anomalies

In some aspects, water behaves differently than most other liquids. First of all, its widely known density anomaly at $4°C$ has many consequences. For example is allows many fish and amphibia to survive winter under water in lakes and some rivers, since the freezing water does not reach the ground of the waterbody and also acts as a protecting sheet on its surface.

2.2.1 Two liquids hypothesis

There are some hypotheses trying to explain waters anomalous behaviour. One of these theories is assuming two different structures in liquid water, which have different densities and are therefore called HDL (high density liquid) and LDL (low density liquid). For a wide temperature and pressure range these two phases coexist, as depicted in figure 1.2. This behaviour is explained by hydrogen bonds, which show a temperature dependent and directional interaction, resulting in different structures within the liquid. This effect is especially important for water molecules, since a water molecule has 'a lot of hydrogen bonding for such a small molecule'[4] and becomes more present, in respect to other molecular forces, for lower temperatures. The lower density configuration is less ordered and has a tetrahedral structure. Whereas the higher density configuration distorts the hydrogen bonding, resulting in weaker and more undirected molecular interactions.[5] John Russo et al. were able to strengthen this hypothesis by modelling water molecules with variable hydrogen bonding. By weakening the hydrogen bonds most of waters anomalies disappeared, implying that hydrogen bonds play an important role in regards to waters anomalies.[6][8]

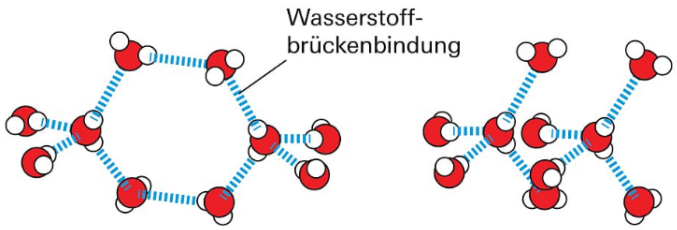

Figure 2.1: Structure of LDL-(left) and HDL-water(right)[12] with hydrogen bonds. The LDL configuration can be viewed as a tetrahedral structure with a water molecule at its center and corners, bonding with another identical tetrahedral structure on an edge (i.e. two hydrogen bonds from one tetrahedra to another one), whereas the HDL structure bonds with another tetrahedra solely from on one corner to the center of another tetrahedra surface (i.e. only one hydrogen bond from one tetrahedra to another one).

The different structures of HDL and LDL water a shown in figure 1.1.

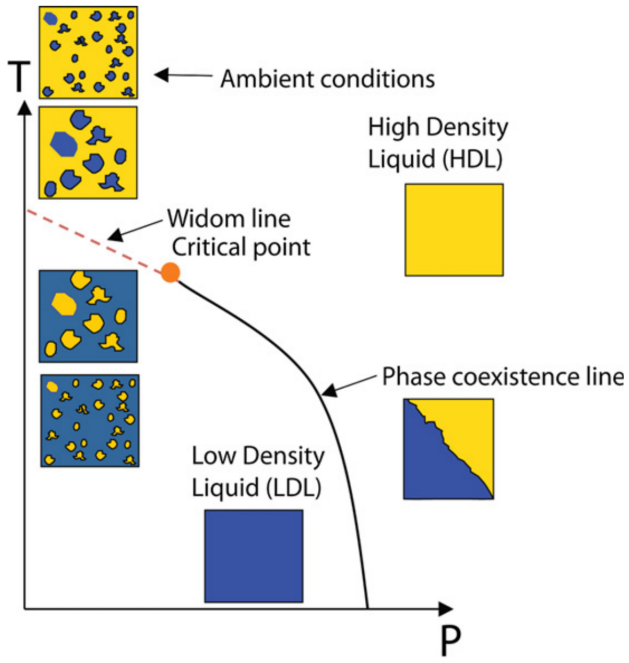

Fig. 10. Schematic picture of a hypothetical phase diagram of liquid water consistent with the observed enhanced scattering at low Q and the structural bimodality indicated by X-ray spectroscopies. Only the liquid–liquid coexistence line, the LLCP and the Widom line are shown for simplicity.

Figure 2.2: In figure 10 of [9] a schematic phase diagram of water with the phase coexistence line as well as the Widom line of LDL and HDL is shown. The Widom line separates liquid-like and gas-like regimes of a supercritical fluid.[9][10][11]

Chapter 3

Model

Molecular and atomic interactions have a wide range of characteristic time-intervals/frequencies and can act up to an infinite distance. To compute those interactions the molecular geometries and interacting forces are approximated with models described in this chapter. For example for this project one can neglect gravitational and nuclear forces, since the main part - by many magnitudes - for intermolecular and -atomic interactions are influenced by electromagnetic potentials. More details on molecular dynamics simulation will be discussed in the following chapter 3.1.1.

3.1 TIP4P/2005

The water model TIP4P/2005 has already been studied thoroughly.[21][25][15] So there already exists a lot of knowledge and data about it that can help us estimate the range of our results as well at their consistency with the work of others.[29][30]

3.1.1 Structure and Properties

The model used for the simulations is TIP4P/2005. The geometric structure of this model is illustrated in figure 2.1 and the geometrical and physical properties are listed in table 2.1. As shown in table 2.1 all the distances and angles of the model are fixed, making it a so called stiff molecule.

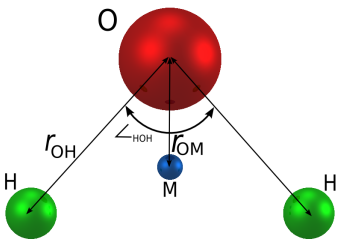

Figure 3.1: Schematic structure of TIP4P/2005 water molecule[18] .

$$U(r)_{LJ_{OO}} = 4\epsilon_{LJ_{OO}} \left[\left(\frac{\sigma_{LJ_{OO}}}{r_{OO}} \right)^{12} - \left(\frac{\sigma_{LJ_{OO}}}{r_{OO}} \right)^{6} \right] \tag{3.1}$$

$$U_{electrostatic} = \frac{e^2}{4\pi\epsilon_0} \sum_{a,b} \frac{q_a q_b}{r_{ab}} \tag{3.2}$$

The electrostatic potential $U_{electrostatic}$ between molecules i and j is described by equation 2.2, where e is the proton charge, ϵ_0 is the permittivity of vacuum, and a and b stand for the charged sites of molecules i and j, with values given in table 2.1, respectively.

r_{OH} [Å]	$\angle_{HOH}$ [deg]	ϵk [K]	
0.9572	104.52	93.2	
$q(O)$ [e]	$q(H)$ [e]	$q(M)$ [e]	r_{OM} [Å]
-1,1128	0.5242	-2q(H)	0.1250
m_O [g/mol]	m_H [g/mol]	$\epsilon_{LJ_{OO}}$ [kkcal/mol]	$\sigma_{LJ_{OO}}$ [Å]
15.9994	1.00794	0.18521	3.1589

Table 3.1: Parameters of TIP4P/2005 water molecule in LAMMPS when used with long-range Coulombic solver $pppm/tip4p$ [21] and $unitsstyle = real$. σ and ϵ for LJ of HH and OH are set to 0, since the molecule is 'stiff'. I.e. the distances and angles remain constrained. For particle-particle interaction between two TIP4P/2005 molecules a LJ potential acts with parameters $\epsilon_{LJ_{OO}}$ and $\sigma_{LJ_{OO}}$. The Hydrogen mass m_H and Oxygen mass m_O are relevant for calculating velocities from acceleration through Newton's laws of motion. The charges $q(O)$, $q(H)$ and $q(M)$ are needed to compute electrostatic forces acting between molecules.

The Lennard-Jones potential acting between molecules i and j is described by equation 2.1. This potential only acts between the Oxygen sites of the model. The distance between the oxygen sites equals r_{OO}. The energy parameter $\epsilon_{LJ_{OO}}$ and distance parameter $\sigma_{LJ_{OO}}$ are given in table 2.1.

3.1.2 Melting Point and Density

Depending on the water model that is used the melting point as well as the liquid and ice density can differ quite a lot from experimental data. In [22][Table VI] found that for TIP4P/2005 the melting temperature of for ice Ih at $1bar$ pressure is $252,1K$, which is about $21K$ lower than the experimental value.
The density for liquid $(0,993\frac{g}{cm^3})$ and ice (Ih) $(0,921\frac{g}{cm^3})$ at a pressure of $1bar$ on the other hand are reported to be relatively near the experimental values of $0,999\frac{g}{cm^3}$ and $0,917\frac{g}{cm^3}$ at that same pressure.

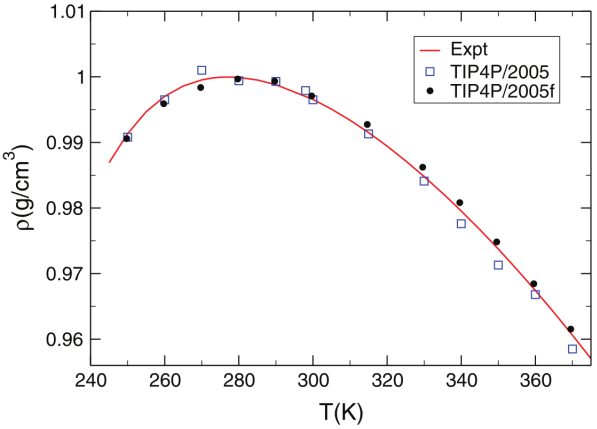

FIG. 3. Densities of the TIP4P/2005f model (full circles) at $p = 1$ bar compared to the values of the same property of TIP4P/2005 model (open squares) and experimental data (full line).

Figure 3.2: In [24] the density of TIP4P/2005 and TIP4P/2005f was computed for different temperatures and plotted together with experimental values for liquid water. TIP4P/2005f is a model described in [24]. The 'f' stands for flexible molecular bonds: a Morse potential for the bond stretching and a harmonic term for the angle bending.

Since water's melting temperature is at about $273K$ the experimental data shown in figure 2.2 seems to correspond to the under-cooled liquid for lower temperatures. Otherwise there would be a visible step to a lower density at the melting temperature as shown in figure 3.3.

3.1.3 Phase Diagram

A phase diagram shows the thermodynamically distinct phases (gas, liquid, solid, crystal structures - if any exist) of a substance/material at thermodynamic equilibrium for distinct thermodynamic properties (for example pressure and temperature). Generally, lines in the phase diagram correspond to states of equilibrium between two phases or phase boundaries. In other words these lines describe, or rather mark, phase transitions. Points at which two (or more) lines intersect are called triple points. They mark conditions at which three (or more) phases can coexist. With knowledge on the phase diagram of the used model one can set the thermodynamic properties to such values that a desired phase occurs at thermodynamic equilibrium.

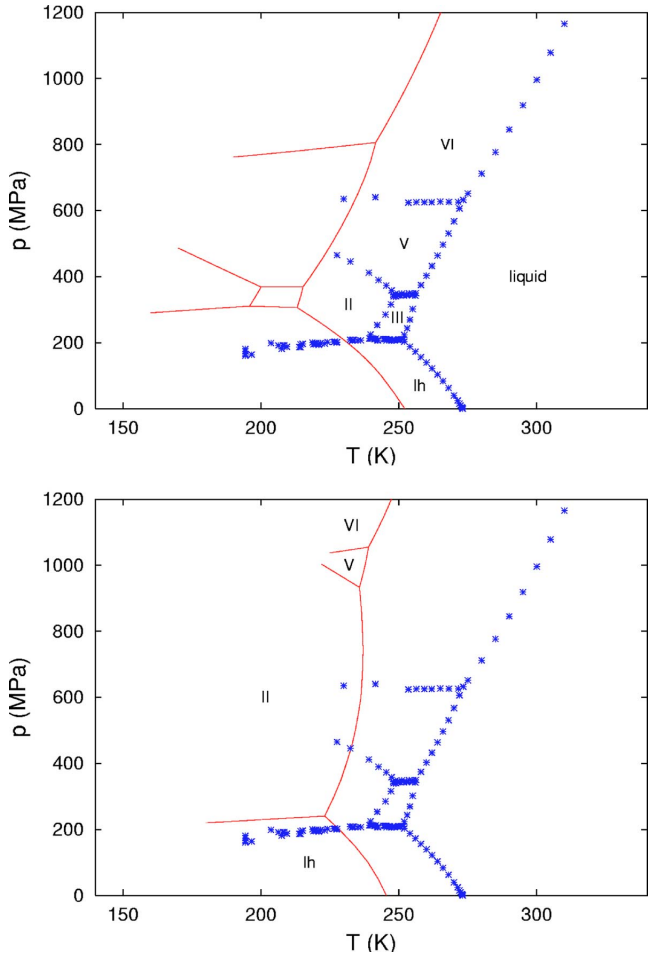

Figure 3.3: In [22] the phase diagram of TIP4P/2005 (upper plot) and TIP4P/Ew (lower plot) was computed. The full lines are the simulation results and the stars the experimental values.

Abascal et al.[22] computed the phase diagram for TIP4P/2005 and TIP4P/Ew using the Monte Carlo method and compared it to the experimental results. In this thesis we will not have a look at the full area of the TIP4P/2005 phase diagram, but rather a constant line with pressure of $1atm$ for a temperature ranging from $250K$ to $280K$.

3.1.4 Diffusion Coefficient

The diffusion coefficient is a measure for the mobility of molecules due to molecular diffusion. For liquids the diffusion coefficient depends on temperature T, Boltzmann constant k_B and the

liquids dynamic viscosity μ. For a multi-species system the diffusion coefficient is given pairwise. For example for CO_2 solved in H_2O it can be written as $D_{H_2O-CO_2}$. The diffusion coefficient has dimensions of $\frac{length^2}{time}$.
More details on the used method to compute it can be found in section 3.7.

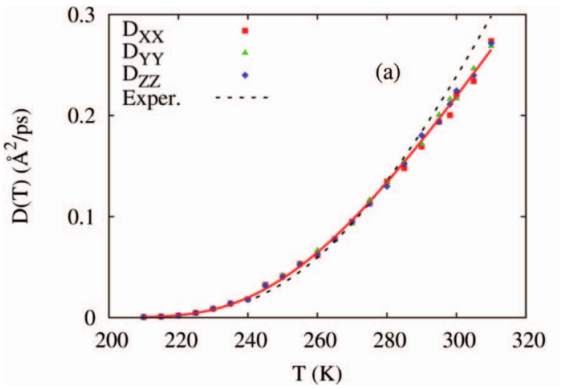

Figure 3.4: Temperature dependent self diffusion coefficient of TIP4P/2005 water[29][30].

As we can see in figure 2.4 for rising temperatures the diffusion coefficient increases. This behaviour is described by [29] and [30] with the following two equations, which are suitable for different temperature ranges, as described below.

$$D(T) = D_0 e^{\frac{-E_D}{RT}} \tag{3.3}$$

$$D(T) = Ae^{\frac{B}{T-T_0}} + C \tag{3.4}$$

Equation 2.3 is suitable for temperatures between $300K$ and $500K$, while equation 2.4 was used to fit data ranging from $210K$ to $310K$. The resulting parameters for equation 2.4 obtained for TIP4P/2005 are shown in figure 2.5[29].

TABLE I. Nonlinear fit parameters for the translational diffusion coefficients of the TIP4P-2005 model of water: for the isotropic diffusion in the world frame, D^{WF}, for the average diffusion in the molecular reference frame, D^{MF}, and for diagonal tensor components in the molecular frame, $D^{\mathrm{MF}}_{\alpha\alpha}$.

	A (Å^2/ps)	B (K)	T_0 (K)	C (Å^2/ps)
D^{WF}	2.799	−314.13	176.76	3.23×10^{-4}
D^{MF}_{xx}	4.099	−418.97	158.58	3.80×10^{-3}
D^{MF}_{yy}	4.386	−368.43	163.72	7.08×10^{-3}
D^{MF}_{zz}	3.641	−414.94	158.41	4.85×10^{-3}
D^{MF}	4.032	−380.62	160.46	5.21×10^{-3}

Figure 3.5: Parameters for diffusion coefficient of TIP4P/2005 water for equation 2.4 found by [29].

3.2 Pore Geometry and Potential Wall

For the experimental set-up in [3], that we tried to reconstruct via computational means, the material containing/confining the water molecules had pores of cylindrical (Vycor) or spherical

(Gelsil) shape. To simulate these pores in our case a potential wall of cylindrical shape, that contains all molecules, was chosen. For the particle-wall interaction a Lennard-Jones potential was chosen. Generally a Lennard-Jones potential is defined as follows:

$$E_{LJ}(r) = 4\epsilon \left[\left(\frac{\sigma}{r_{WP}} \right)^{12} - \left(\frac{\sigma}{r_{WP}} \right)^{6} \right] \tag{3.5}$$

Where σ is the size/distance parameter, ϵ an energy parameter and r_{WP} is the distance between particle and wall. For increasing σ the potential interaction has a longer range and for increasing ϵ the acting force, being determined by the potential slope, also increases.
Using the simulation software LAMMPS command 'fix wall/lj126' [21] (more details about LAMMPS and the used parameters are described in section 3.3) and choosing the cutoff radius r_{cutoff} to be $2^{1/6}$ times the potential cutoff distance we ensure that there are no attractive forces keeping the particles attached to the wall, but only repulsive ones act between particles and the wall. I.e. $r_{cutoff} = r_m$, with r_m being the distance to the wall at which the potential has a minimum. Also the potential is shifted so that it equals zero at the cutoff radius. This way the total energy of the system can only be increased by wall interactions, resulting in the following equation:

$$E_{LJlammps}(r) = \begin{cases} 4\epsilon \left[\left(\frac{\sigma}{r_{WP}} \right)^{12} - \left(\frac{\sigma}{r_{WP}} \right)^{6} + \frac{1}{4} \right] & \text{for} \quad r_{WP} < 2^{1/6}\sigma \\ 0 & \text{otherwise} \end{cases} \tag{3.6}$$

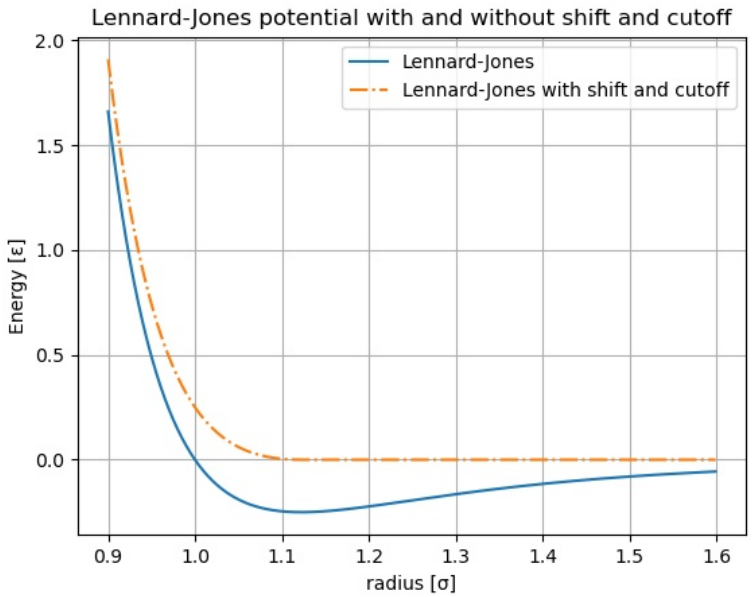

Figure 3.6: Lennard-Jones potential with and without cut-off and shift.

Chapter 4

Methods

In this chapter we will have a look at the methods used to approach the task at hand. The basic concepts of the approach by computational means will be explained, followed by a short overview of the necessary parameters for the simulation software package used as well as some details on how the used simulation software package takes long ranging forces/potentials, which need to be considered in our scenario, into account. After that we will explain how the desired initial configuration of molecules is prepared. Finally the data evaluation methods are explained, including some basic concepts of Brownian motion.

4.1 Why approach the problem with a MD simulation?

Getting porous materials with uniformly distributed pore size and orientation is technically extremely difficult if not (at the moment) impossible. Therefore a structure analysis with diffraction methods cannot be obtained as easily as with a molecular dynamics (MD) simulation. With the means of a molecular dynamics simulation it is also possible to swiftly and easily obtain more information on kinetic processes and therefore determine parameters like the diffusion coefficient, since positions, velocities as well as other ensemble parameters of the simulated atoms/molecules at any given simulation time step can be saved. More details on Brownian motion and the diffusion coefficient can be found in section 3.7.

4.1.1 What is a MD simulation?

In a molecular dynamics simulation one is solving Newton's equations of motion for a system with multiple particles. This is achieved by first expanding the equations of motion with a Taylor series and following approximation by neglecting terms of higher order to save computing power. This neglect comes with the price of losing information on the system by not following its 'true' trajectory in phase space. In most cases this systematic error can be ignored, since it mostly scales with the 4th or higher order of the time step used, resulting in relatively small deviations, as long as the chosen time step is smaller than the period corresponding to the highest frequency.[16] There are many methods that can be implemented, each potentially yielding different results, depending on the systems parameters and size of the time step used.

4.2 Properties of the velocity Verlet-Algorithm

Some important physical properties are provided by the velocity Verlet-integrator. Such as time-reversibility and preservation of the phase space symplecticity. It is also relatively simply implemented and comes with a relatively low memory cost, since only the current positions and velocities are needed to compute the following positions and velocities.

$$\vec{x}(t+\Delta t) = \vec{x}(t) + \vec{v}(t)\Delta t + \frac{1}{2}\vec{a}(t)\Delta t^2 \tag{4.1}$$

$$\vec{v}(t+\Delta t) = \vec{v}(t) + \frac{\vec{a}(t) + \vec{a}(t+\Delta t)}{2}\Delta t \tag{4.2}$$

The acceleration $\vec{a}(t)$ is computed by applying Newton's Laws of Motion:

$$veca(t) = \frac{\vec{F}(t)}{m} \tag{4.3}$$

So one first computes the new positions with equation 3.1, then the previous and current forces, which are derived from the particles positions via acting potentials. By applying Newton's Laws of Motion one then computes the acceleration from the forces with equation 3.3 and can thus get the velocity for the new (i.e. current) time step with equation 3.2.
The positions local error for the Verlet integrator is of 4th order in the time step, whereas the local error for the velocity scales in the time steps 2nd order.

4.2.1 RATTLE Algorithm

As mentioned in section 2.1.1 for our chosen model the water molecule has a stiff geometry, so called constraints. To compute those constraints a RATTLE algorithm was chosen. Similar to SHAKE, it is based on the integration of the equations of motion via velocity Verlet algorithm. With the RATTLE algorithm, the positions and velocities of the particles (in our case TIP4P/2005 water molecules) at the next time step are computed from the present time steps velocities and positions. Since no information on the previous time steps is needed, this algorithm needs less memory than other methods would. Another advantage is the use of Cartesian coordinates for the atoms constraints, simplifying the algorithms implementation.[26]

4.3 LAMMPS

The molecular dynamics program LAMMPS[21] (Large-scale Atomic/Molecular Massively Parallel Simulator), from Sandia National Laboratories, was used to create all ensembles discussed in this thesis.
In the following subsection the chosen parameters will be discussed.

4.3.1 Long Range vs. Short Range (cut-off) - kspace

A long range solver for LAMMPS was chosen. This way each timestep long-range Coulombic interactions and long-range interactions scaling with r^{-6} are not being neglected. With LAMMPS kspace command these interactions are solved in k-space with a fast Fourier transform (FFT). For this solver the effective cut-off distance for Coulombic (or other r^{-N}) interactions is infinite. For our simulation this implies an infinite number of simulation boxes stacked over one another, repeating the molecular configuration of the 'original' volume periodically in one dimension, i.e. periodic boundary conditions are applied.
The chosen style $pppm/tip4p$ for the LAMMPS command $kspace\_style$ invokes a particle-particle particle-mesh solver [27], which the molecules charges to a 3d mesh and then solves Poisson's equation on the mesh by means of FFTs. Then electric fields are interpolated on the mesh points back to the atoms.
Another method would be to solve it traditionally via Ewald summation, which scales by $N^{3/2}$, where N is the number of atoms in the system. Due to the FFTs the PPPM solver scales by $Nlog(N)$. As consequence the PPPM solver is almost always faster, saving us valuable computing time.

The difference between the $pppm/tip4p$ style and the $pppm$ style is that in $pppm/tip4p$ a charge is added at the mass-less 4th site in each TIP4P water molecule.
The accuracy equals the desired relative error in forces.[21]
pppm/tip4p value = accuracy
For the final configuration described in chapter 3.4 the Ewald-sum is computed for the case of periodic boundaries in all directions.

4.4 State Preparation

As initial configuration an Ih-ice cube with about 786 molecules is chosen.

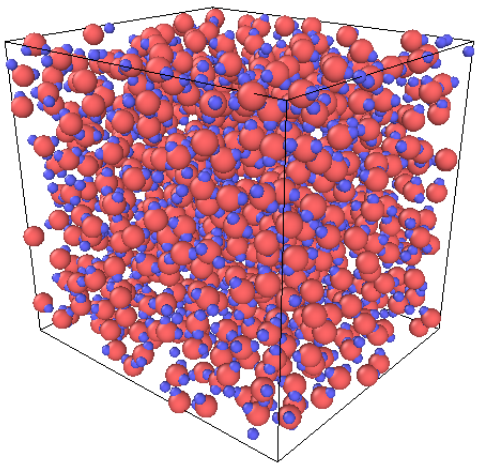

Figure 4.1: Ih-ice structure in cubic volume containing 786 TIP4P/2005 molecules.

That initial configuration is replicated in all three spatial dimensions, leading to a cuboid box volume. This way we get much larger configurations with 12000 to 50000 molecules, depending on the desired final pore size. The ice is then melted as a NVT-ensemble at $300K$ to obtain a liquid configuration. After reaching thermodynamic equilibrium the liquid water is cooled down as a NpT-ensemble in order to obtain a supercooled liquid. Supercooled liquids are liquids with a temperature lower than their freezing point at a given pressure, but still in their liquid phase. Now, having a cuboid structure of supercooled water molecules, we need to create our desired geometry: a cylinder volume filled with water molecules. So the obvious next step is to delete all water molecules from our position file that are not included in our cylinder with radius r_c and to add a potential wall.

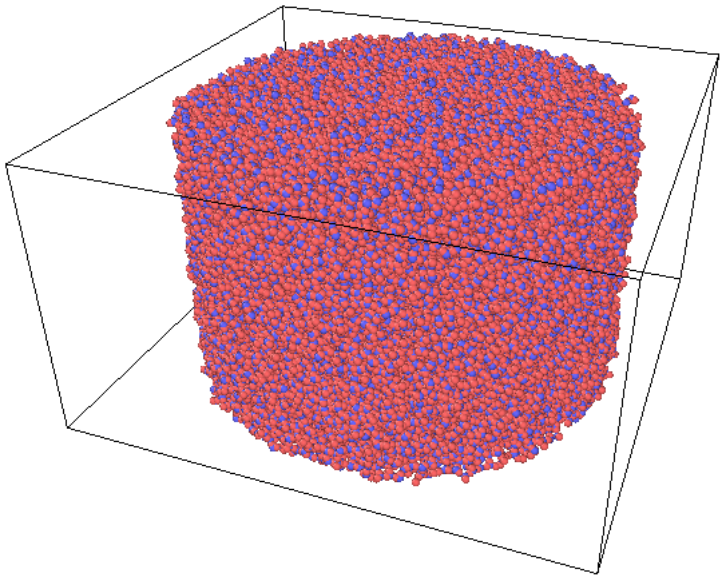

Figure 4.2: Cuboid volume with cylinder structure with radius r_c of $69.26\mathring{A}$ containing 40407 TIP4P/2005 molecules at $275K$.

With this final cylinder configuration only periodic boundary conditions parallel to the cylinder axis are implemented for the motion of the particles.

4.5 Density Distribution $\rho(r_N)$

To get a better understanding of wall effects we have a look the density distribution $\rho(r)$ in respect to the distance r from the cylinders axis. For that we simply divide our cylinder in segments of equal thickness. The area A_N and volume V_N of cylinder segment N, for a cylinder with radius r_c divided in Z parts with equal thickness $r_Z = \frac{r_c}{Z}$:

$$A_N = r_Z^2 \pi (2N - 1) \quad \text{for } N \in \{1, 2, ..., Z\} \tag{4.4}$$

$$V_N = r_Z^2 \pi h (2N - 1) \quad \text{for } N \in \{1, 2, ..., Z\} \tag{4.5}$$

To compute the radius depending density $\rho(r_N)$ for a cylinder segment with outer radius $r_N = N r_Z$ we count the number of molecules N_N contained in volume V_N, multiply it with the mass of one water molecule and divide it by the volume V_N of the corresponding cylinder segment.

$$\rho(r_N) = \frac{m_{H2O} N_N}{V_N} \quad \text{for } N \in \{1, 2, ..., Z\} \tag{4.6}$$

With the density we may be able to get an indication if the water is in liquid or solid state. This is due to the fact that the macroscopic density for liquid water at temperature $277,13K$ and pressure of $1bar$ is $1\frac{kg}{dm^3}$, varying by less than 1% for the liquid phase up until about $317K$ and a relatively large step to about $0,92\frac{kg}{dm^3}$ when freezing at about $273K$ to the hexagonal I_h structure.
With this parameter we may be able to observe wall effects regarding liquid and solid phase. For further investigations on the phase it may be necessary to look at hydrogen bonds. Investigations on hydrogen bonds will not be covered in this thesis.
In [22] the density for the water model TIP4P/2005 varies form $0,9908\frac{kg}{dm^3}$ to $1,0010\frac{kg}{dm^3}$ in the range of $250K$ to $290K$, as one can see in figure 2.2.

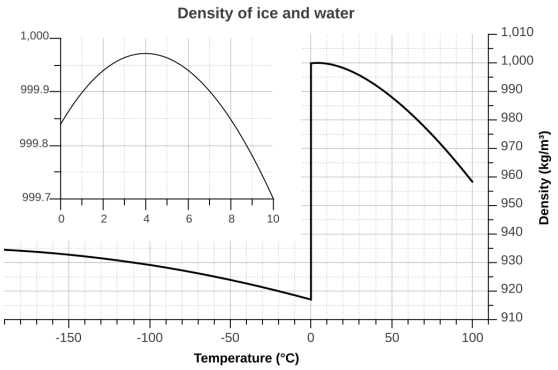

Figure 4.3: Density of ice and water for a temperature ranging from $100K$ to $373K$. One can clearly see the density jump for the phase transition from liquid water to solid ice.[37]

With the mass of a water molecule of $2.9915 \cdot 10^{-23}g$ and a density of $1\frac{kg}{dm^3}$ one can easily compute the mean volume occupied by a single water molecule $\bar{V}_{H2O}$:

$$\bar{V}_{H2O} = \frac{2,9915 \cdot 10^{-23}g}{1\frac{kg}{dm^3}} = 29,915\mathring{A}^3 \tag{4.7}$$

4.6 Pair Correlation Function $g(r)$

The pair correlation function (or radial distribution function) describes how density varies as a function of distance from a reference particle. It is calculated by counting how many particles are found in a spherical shell of thickness dr and radius r around a particle and then normalizing it by dividing it by the macroscopic density ρ and the spherical shells volume $4\pi r^2 dr$.

$$g(r) = \frac{n(r+dr)}{\rho 4\pi r^2 dr} \tag{4.8}$$

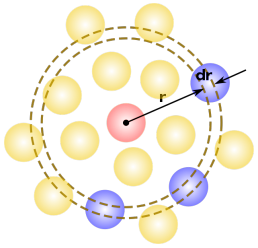

Figure 4.4: Schematic description of pair correlation function.[38] The number n corresponds to the of particles (blue) in the sphere shell with radius r and thickness dr around the central (red) particle.

In our case the radius r equals r_N and dr equals r_Z.
For sufficiently large distances r_N the fraction of number of particles N_N found in the spherical shells volume V_N divided by the shells volume V_N converges to the macroscopic particle density ρ. Therefore the pair correlation function $g(r)$ converges to 1 for growing r, as one can see in the following plots. For a system of spherical particles with equal diameter the first maximum in the plots corresponds to about the particle diameter. The maxima and minima can give a hint if the configuration is liquid or crystalline, as depicted in different figures 3.5 to 3.8.

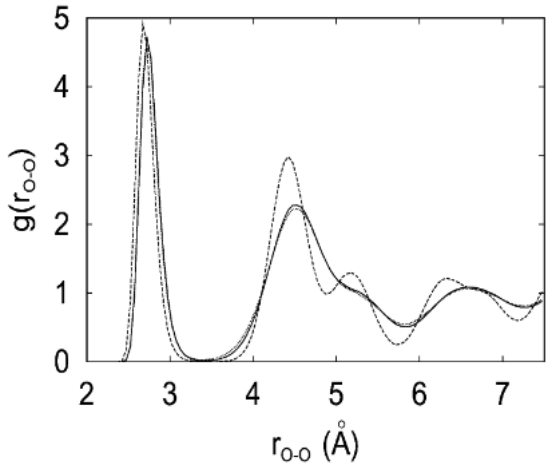

Fig. 3 Oxygen–oxygen site–site distribution function for ice I_h at 250 K and 0 GPa. TIP4P solid line, TIP5P dashed line and SPC/E dotted line.

Figure 4.5: Pair correlation function of crystalline ice I_h structure for different water models at $250K$ and $0GPa$.[23]

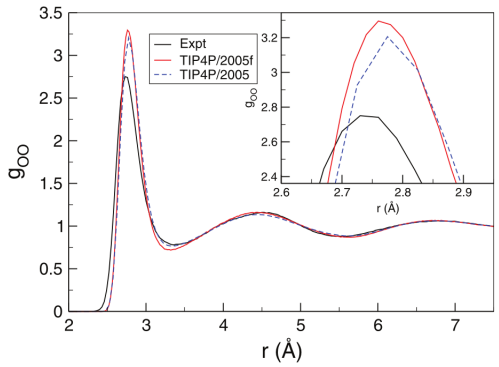

FIG. 4. Oxygen-oxygen radial distribution function at $T = 298$ K, $p = 1$ bar.

Figure 4.6: In figure 4 of [24] the oxygen-oxygen pair correlation function at 295K and 1bar for experimental and simulation data is shown. TIP4P/2005f is a model described in [24]. The 'f' stands for flexible molecular bonds: a Morse potential for the bond stretching and a harmonic term for the angle bending.

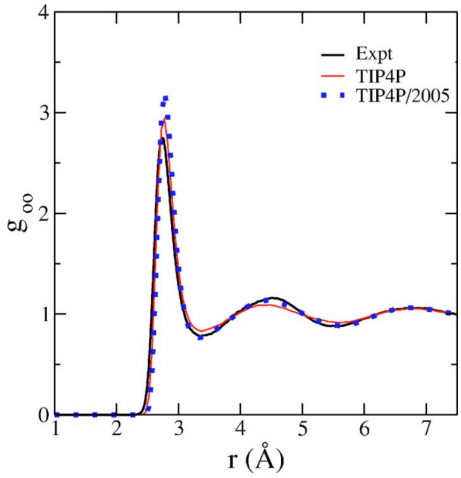

FIG. 8. Oxygen-oxygen correlation function at 298 K. Thick (black) line: Experimental data (Ref. 38); thin (red) line: TIP4P; dotted (blue) line: TIP4P/2005.

Figure 4.7: In figure 8 of [22] the oxygen-oxygen pair correlation function at 298K for experimental and simulation data is shown.

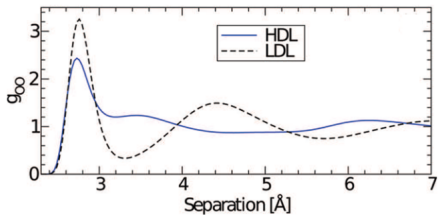

Figure 5. Radial oxygen−oxygen pair-distribution functions for HDL and LDL demonstrating the structural difference between high- and low-density water at ambient temperature. Adapted with permission from ref 67. Copyright 2000 by the American Physical Society.

Figure 4.8: In figure 5 of [6] the oxygen-oxygen pair correlation function for LDL and HDL at ambient temperature is shown. The reference 67 mentioned under the plot is [7].

4.7 Brownian Motion and Mean Square Displacement - MSD

The Mean Square Displacement (MSD) is calculated by squaring the distance from a starting point $x(0)$. From the MSD one can compute the diffusion of particles performing Brownian motion in n dimensions coefficient by the following equation[28]:

$$MSD(t) =< (x(t) - x(0))^2 >= 2nDt \tag{4.9}$$

Equation 3.9 can be transformed to get an expression for the diffusion coefficient D either in terms of the mean square displacement or the velocity autocorrelation:

$$D(t) = \frac{1}{2n}\frac{d}{dt} < (x(t) - x(0))^2 >= \frac{1}{n}\int_0^t dt' < v(t')v(0) > \tag{4.10}$$

For liquids whose molecules perform Brownian motion the Diffusion constant D depends on the absolute Temperature T, the Boltzmann constant k_B and the dynamic viscosity μ. This is described by the Einstein relation [28]:

$$D = \mu k_B T \tag{4.11}$$

With these descriptions of diffusion processes we can easily derive the diffusion coefficient from the MSD slope and compare our results to those from [29][30][32][33].

4.7.1 Ballistic regime

For small time steps and temperatures the probability of not interacting with another molecule is relatively high, since there is some free space between the molecules. So during that time the molecules move at a relatively constant speed, resulting in a quadratic MSD. This leads to a seeming jump in the MSD, before passing over to a linear slope. If one chooses a small enough time interval for the MSD plot and a small enough time step this transition is clearly discernible. This transition is clearly visible in figure 4.7 in chapter 4.3.

4.7.2 Box size affecting diffusion

The size of the simulation box affects the diffusion coefficient and other model properties. The diffusion coefficient scales with $N^{-\frac{1}{3}}$[31] [32] [34] [35]. For our simulations this effect should not be relevant, since the volume is large enough for all configurations shown in the results section below.

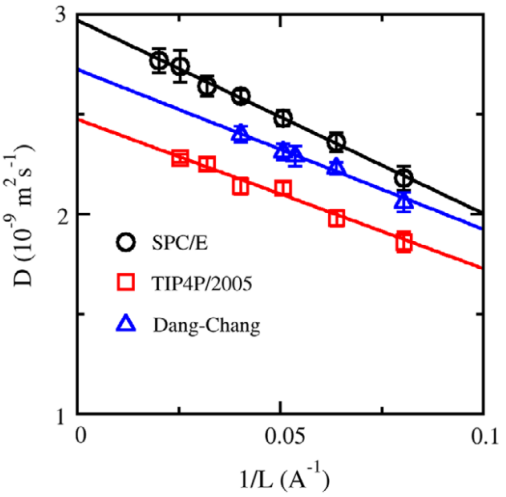

Figure 1. Diffusion coefficient as a function of the inverse box size. The size-independent diffusion coefficient D_0 is the extrapolation at $1/L \to 0$. The slope provides an estimate of the viscosity η_{PBC} using equation (2).

Figure 4.9: In [35] it was shown that the diffusion coefficient for different rigid water models depends on the simulation box size.

In [35] the equation for system size depending diffusion coefficient for periodic boundary conditions D_{PBC} in terms of box length L is given as follows:

$$D_{PBC} = D_0 - \frac{2.837 k_B T}{6\pi\eta L} \tag{4.12}$$

With D_0 being the bulk diffusion coefficient, Boltzmann constant k_B, temperature T and viscosity η.

Chapter 5

Results

In this chapter the results from the different evaluation methods from chapters 3.5 3.6 and 3.7 will be presented and discussed.
The different box parameters for the cylinder configurations are listed in table 4.1.
For all of those cylinder configurations the temperature was set to values listed in table 4.2. With the three different cylinder geometries and seven temperatures we get a total of 21 cylinder NVT-ensembles.
Additionally a NVT-ensemble of a periodic cube with box diameters of about $(110 \times 125 \times 117)\mathring{A}^3$ and 49512 molecules with a temperature of $300K$ has been simulated, to get a reference for the pair correlation function.
To show the ballistic regime mentioned in chapter 3.7.1 a cylinder NVT-ensemble with a temperature of $285.2K$, 55840 molecules, radius $r_C = 63\mathring{A}$ and height $h = 144.3\mathring{A}$ and periodic boundaries in z-direction was simulated for a total time of $1ps$ by saving positions for a time step of $20fs$.
Another two cubic volumes with periodic boundary conditions containing 49152 TIP4P/2005 molecules have been simulated as NpT-ensemble ($1bar$) and NVT-ensemble ($(100 \times 120 \times 115)\mathring{A}^3$) at a temperature of $330K$, to compute their diffusion coefficient via the MSD and compare it to results from [29], [30], [32] and [33].

number molecules	cylinder radius r_C	cylinder height h
10427	$28.5\mathring{A}$	$138.1\mathring{A}$
14075	$41.6\mathring{A}$	$84.9\mathring{A}$
40407	$69.3\mathring{A}$	$86.1\mathring{A}$

Table 5.1: Box sizes and corresponding number of molecules for presented results in cylinder configurations.

$250K$	$255K$	$260K$	$265K$	$270K$	$275K$	$280K$

Table 5.2: Temperatures used for cylinder configurations listed in table 4.1.

mass	distance	temperature	energy	velocity	force	torque
g/mol	$\mathring{A}$	K	$kcal/mol$	$\mathring{A}/fs$	$kcal/(mol * \mathring{A})$	$kcal/mole$
time	pressure	dyn. viscosity	charge	dipole	electric field	density
fs	atm	$Poise$	e	$e * \mathring{A}$	$V/\mathring{A}$	$gram/cm^{dim}$

Table 5.3: Units for LAMMPS[21] real style.

5.1 Density Distribution

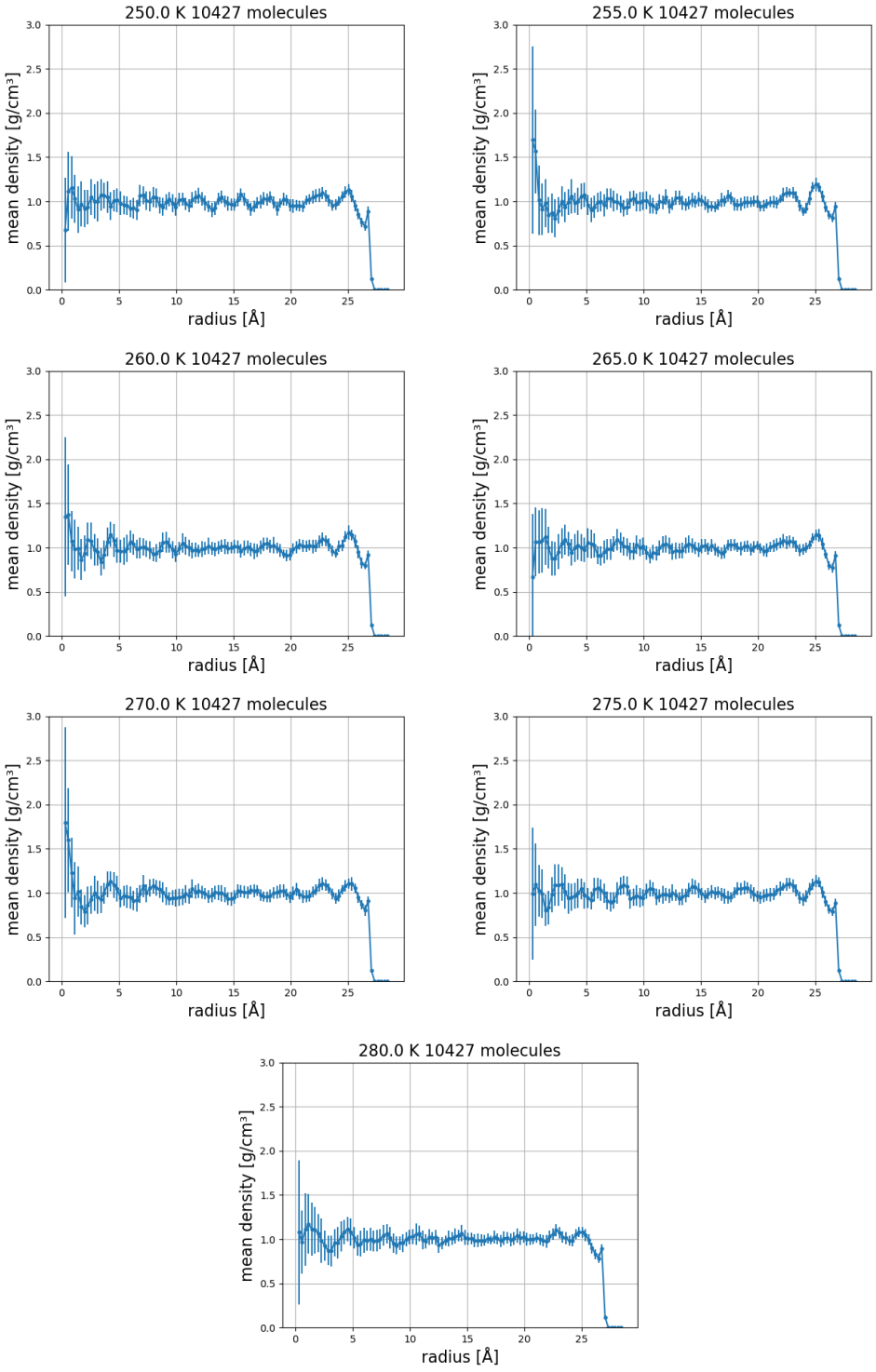

Figure 5.1: Mean radial density distribution at various temperatures for NVT-Ensembles of 10427 water (TIP4P/2005) molecules in cylinder volume with periodic boundary in z-direction and a radius of $28.5\mathring{A}$ for different temperatures averaged over the last $20ps$ of a runtime of $400ps$.

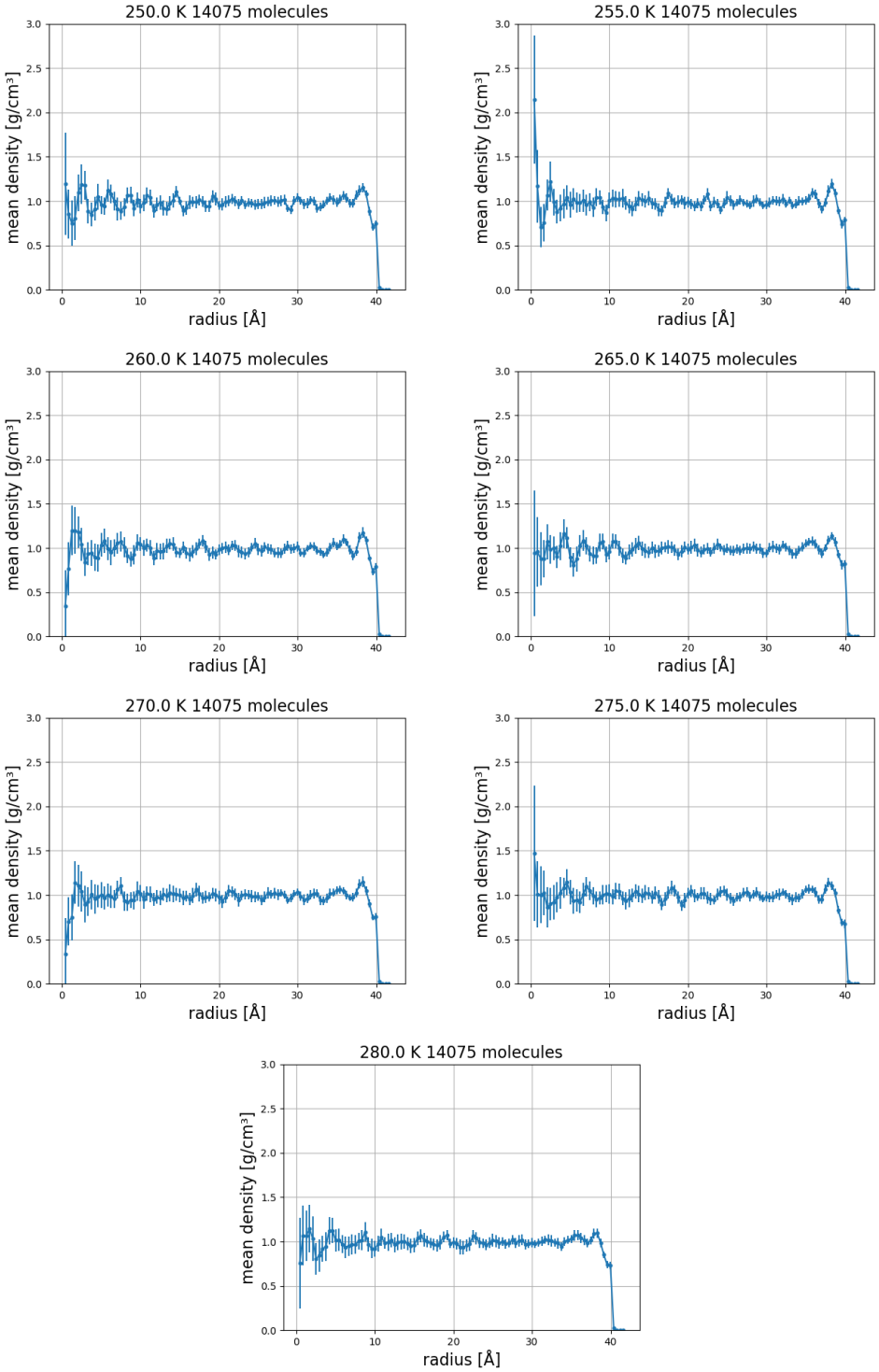

Figure 5.2: Mean radial density distribution at various temperatures for NVT-Ensembles of 14075 water (TIP4P/2005) molecules in cylinder volume with periodic boundary in z-direction and a radius of $41.6\mathring{A}$ for different temperatures averaged over the last $20ps$ of a runtime of $400ps$.

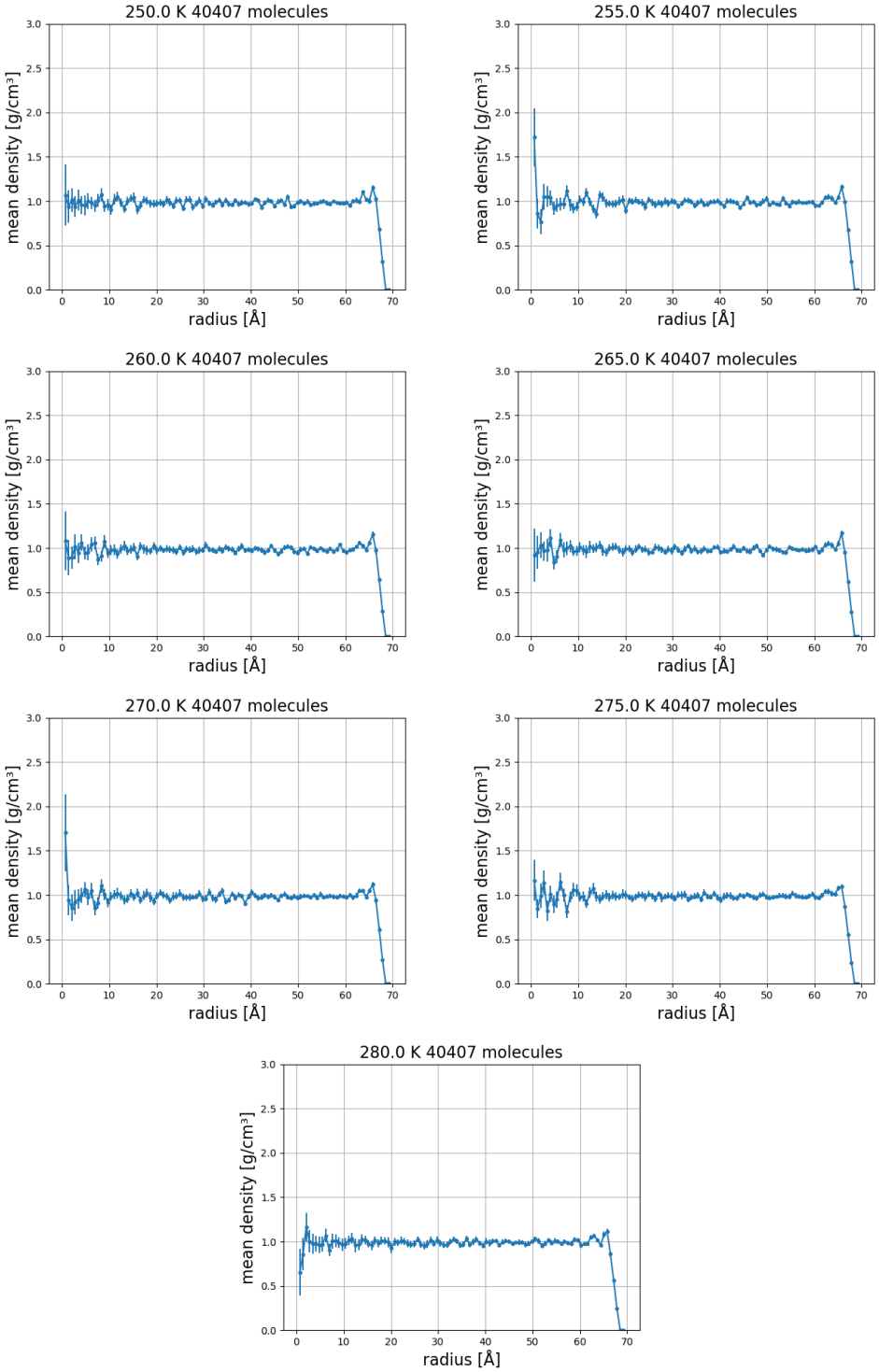

Figure 5.3: Mean radial density distribution at various temperatures for NVT-Ensembles of 40407 water (TIP4P/2005) molecules in cylinder volume with periodic boundary in z-direction and a radius of $69.2\mathring{A}$ for different temperatures averaged over the last $20ps$ of a runtime of $400ps$.

In figures 4.1 to 4.3 the radial density distribution of the last $20ps$ of NVT ensembles with a total runtime of $400ps$ were evaluated for different sample sizes and temperatures. The relatively large standard deviation for small radii results from the comparatively small number of molecules inside the inner cylinder shells that move from one shell to another. It is visible in all figures that the density does not deviate significantly from the density of bulk liquid water. This agrees with the data from figure 2.2 from [24]. The wall potential cut off of $2\mathring{A}$ affecting the density is also visible. None of the figures seem to indicate frozen configurations, which would have a significantly lower density. This agrees with the the data from figure 2.2 reported by [22], indicating that the used model freezes at lower temperatures.

5.2 Pair Correlation Function

In figures 4.4 to 4.6 the pair correlation function for all ensembles is plotted together with the pair correlation function of a NVT-ensemle with periodic boundary conditions of 49152 particles with a temperature of $300K$ and box diameters of about $(110 \times 125 \times 117)\mathring{A}^3$.

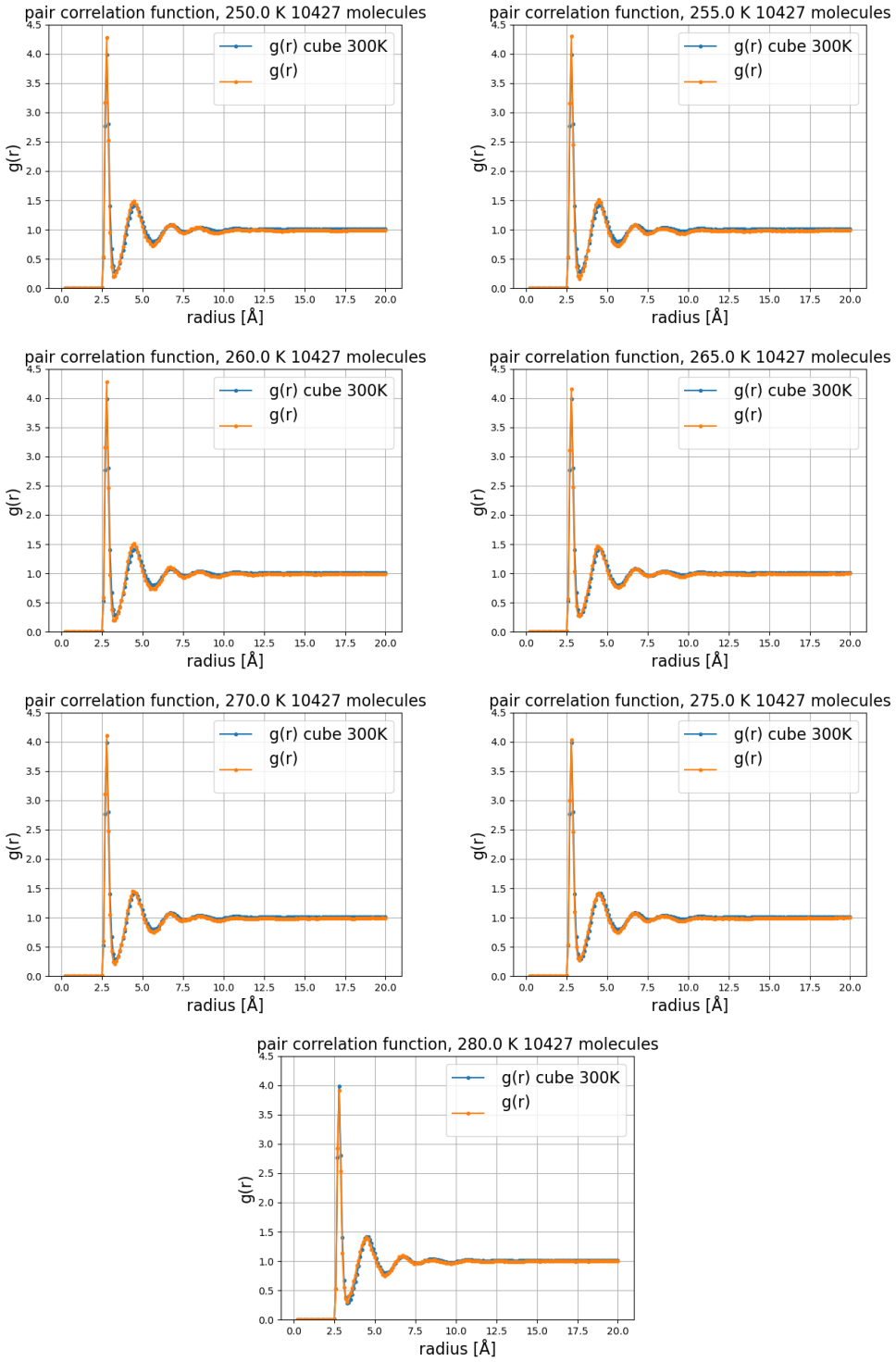

Figure 5.4: Pair correlation function $g(r)$ for NVT-Ensembles of 10427 water (TIP4P/2005) molecules in cylinder volume with periodic boundary in z-direction and a radius of $28.5\mathring{A}$ for different temperatures averaged over the last $20ps$ of a runtime of $400ps$ and a periodic cube with a NVT-ensemle with a temperature of $300K$ and box diameters of about $(110 \times 125 \times 117)\mathring{A}^3$.

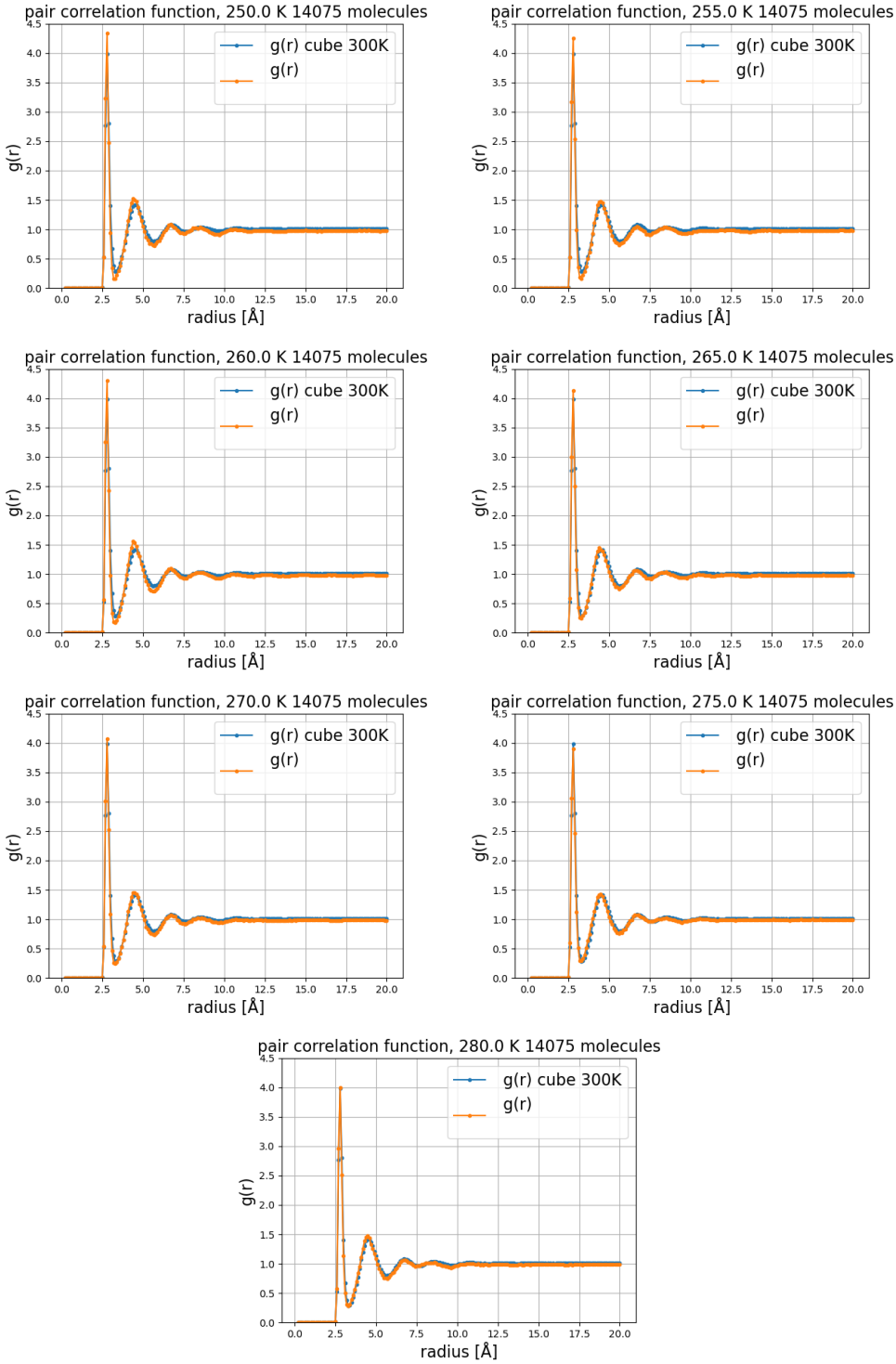

Figure 5.5: Pair correlation function g(r) for NVT-Ensembles of 14075 water (TIP4P/2005) molecules in cylinder volume with periodic boundary in z-direction and a radius of $41.6\mathring{A}$ for different temperatures averaged over the last $20ps$ of a runtime of $400ps$ and a periodic cube with a NVT-ensemle with a temperature of $300K$ and box diameters of about $(110 \times 125 \times 117)\mathring{A}^3$.

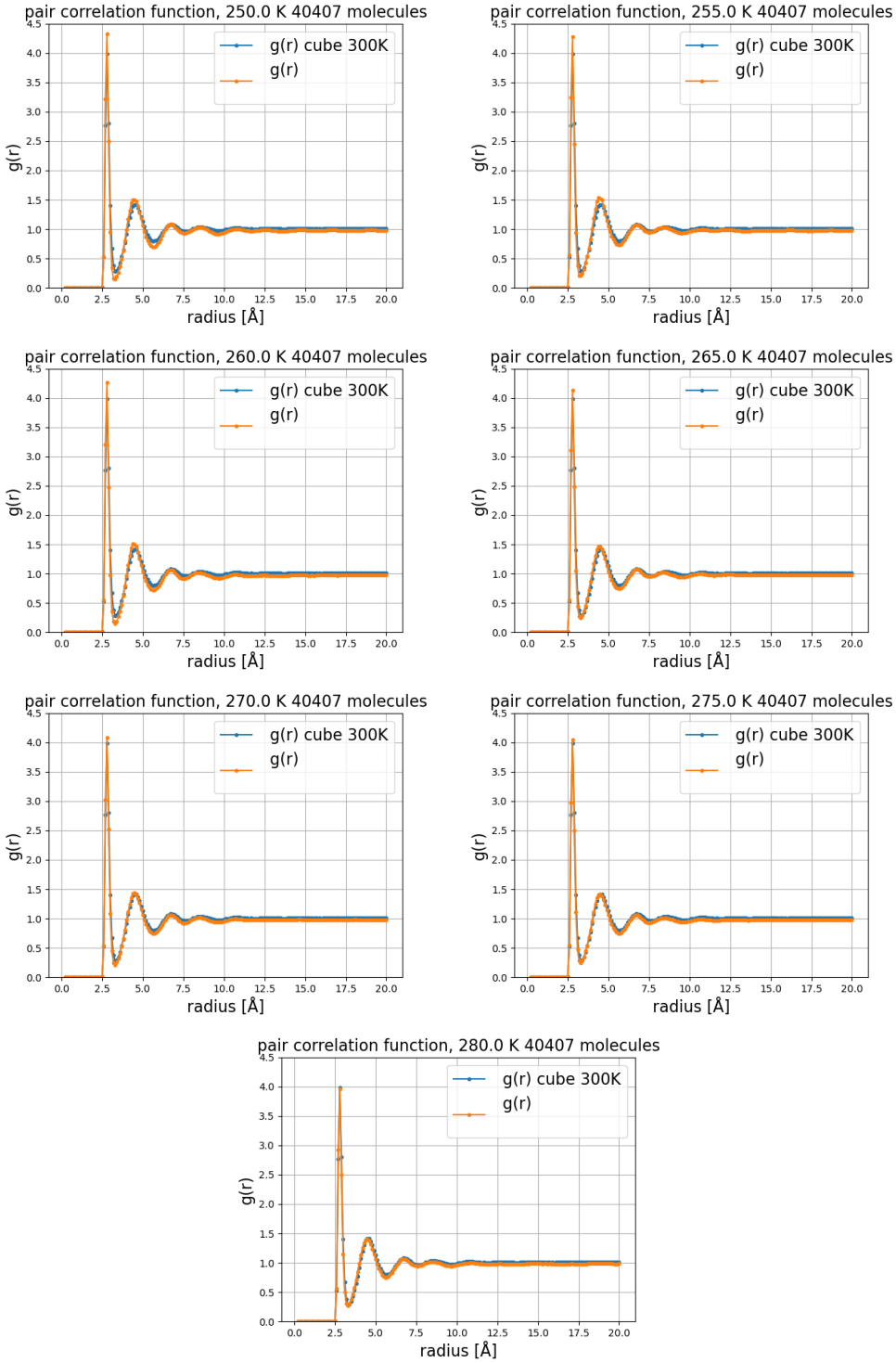

Figure 5.6: Pair correlation function g(r) for NVT-Ensembles of 40407 water (TIP4P/2005) molecules in cylinder volume with periodic boundary in z-direction and a radius of $69.3\mathring{A}$ for different temperatures averaged over the last $300ps$ of a runtime of $400ps$ and a periodic cube with a NVT-ensemle with a temperature of $300K$ and box diameters of about $(110 \times 125 \times 117)\mathring{A}^3$.

In figures 4.4 to 4.6 the pair correlation function for all ensembles is plotted together with the pair correlation function of a periodic cube containing 49152 molecules with a temperature of $300K$ and box size of about $(110 \times 125 \times 117)\mathring{A}^3$. It was computed for molecules initially positioned at the cylinder axis to a maximum distance to it of 20% of the cylinders radius. In all these figures the first maximum is up to about 50% higher than reported in figures 3.6[24] 3.7[22] 3.8[6]. At least the position of the maxima and minima seems to correspond to the reported data. When comparing it to 3.8 it seems as if the overall configuration for all ensembles is more similar to the LDL structure than the HDL one.

5.3 Mean Square Displacement - Ballistic Regime

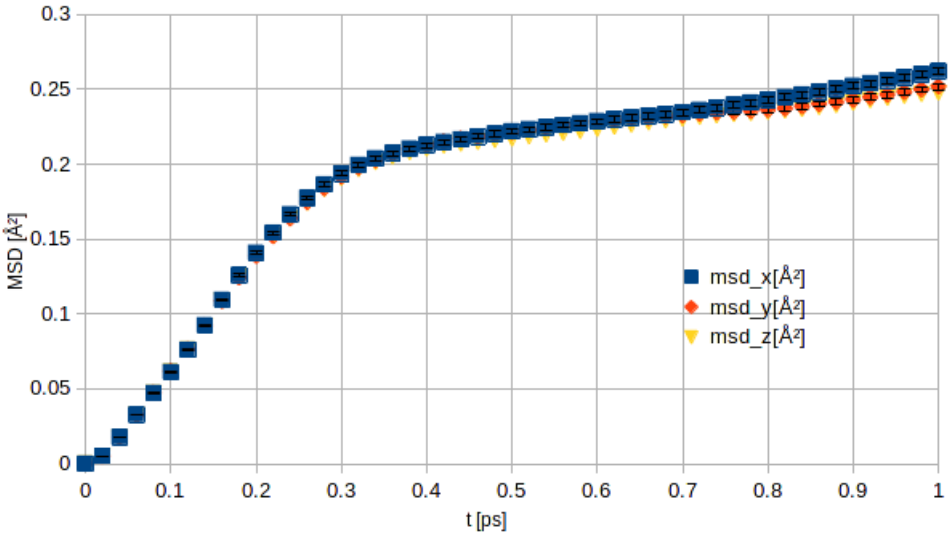

Figure 5.7: MSD for time steps of $20fs$, showing the 'ballistic regime' in three dimensions for Cartesian coordinates (msd_x, msd_y and msd_z), ranging from $0ps$ to $1ps$. The temperature for this NVT-Ensemble was set to $285,2K$, with 55840 water (TIP4P/2005) molecules in a cylindic volume with periodic boundary in z-direction and a radius of $63\mathring{A}$.

In figure 4.7 one can clearly observe the transition from the ballistic regime to the regime of diffusion described by equations 3.9 to 3.11. In figure 4.7 the boundary conditions have no visible influence on the MSD on the chosen time scale, since the molecules don't have enough time to interact with the potential wall for an ensemble this big to influence their overall movement. Also the periodic box size effects can be neglected for a time scale this small and for the relatively large chosen volume [32]. Even the enclosing cylinder potential wall has no immediate visual effect on the ballistic regime, since the MSD has the same shape for all three perpendicular directions of the Cartesian coordinates.

5.4 Mean Square Displacement

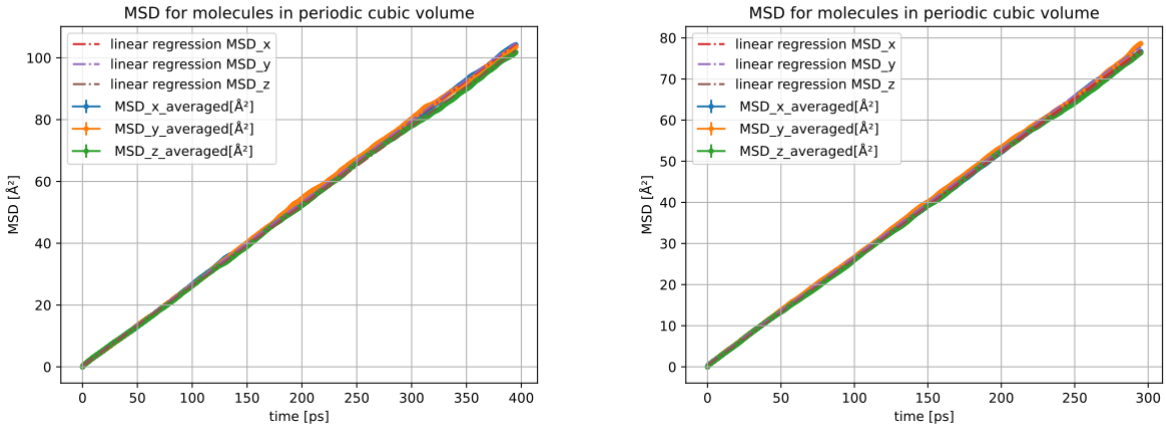

Figure 5.8: MSD 49152 water (TIP4P/2005) molecules in a cubic volume of $(100 \times 120 \times 115)\mathring{A}^3$ with periodic boundaries and a time step of $500fs$ in three dimensions. The temperature for these ensembles was set to $330K$. The pressure for the NpT-ensemble (left) was set to $1bar$. The NVT-ensemble (right) was computed starting with the last step of the NpT-ensemble.

In figure 4.8 the diffusion coefficient was derived for an NpT (left) and NVT (right) ensemble of 49152 TIP4P/2005 water molecules in a cube of about $(100 \times 120 \times 115)\mathring{A}^3$ and periodic boundary conditions at a temperature of $330K$. The diffusion coefficient derived from the MSD via linear regression equals about $0,125\frac{\mathring{A}^2}{ps}$ for both ensembles and is about four times lower than the values reported in [29], [30], [32] and [33]. After some investigation and comparison from the data evaluation scripts with the MSD data provided by LAMMPS, which only gave the MSD averaged over all particles, and having a look at density distribution as well as pair correlation it was still unclear what effects causes this apparent decrease in diffusion. Also the mean kinetic energy corresponds to the expected value of $\frac{6}{2}k_BTN$ for all simulations.

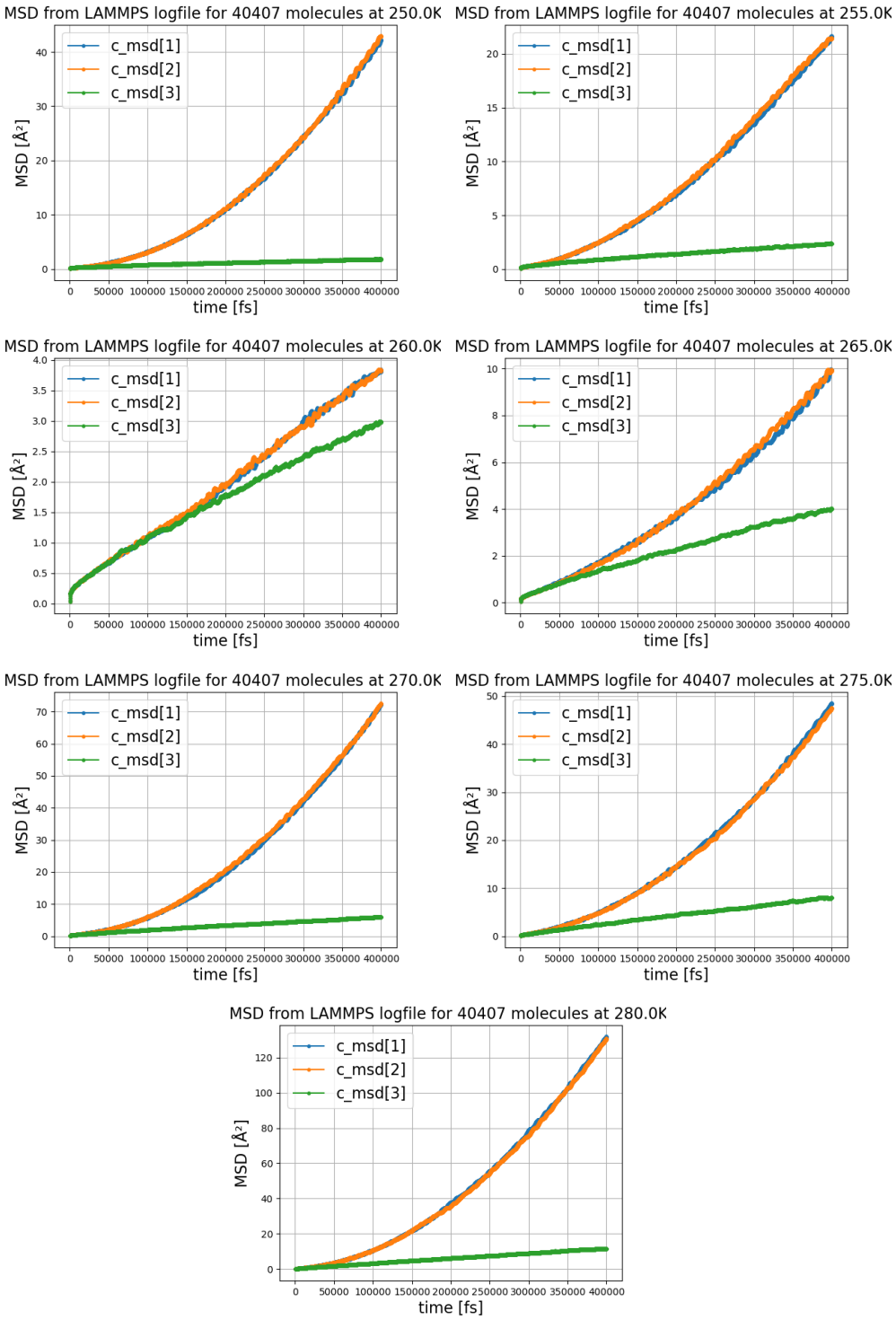

Figure 5.9: MSD from LAMMPS logfile for NVT ensemble in cylinder radius of about $69.2\mathring{A}$ with 40407 molecules and periodic boundaries in z-direction for different temperatures.

In the following figures the range indicates the molecules initial position in $\%$ of the cylindric wall radius.

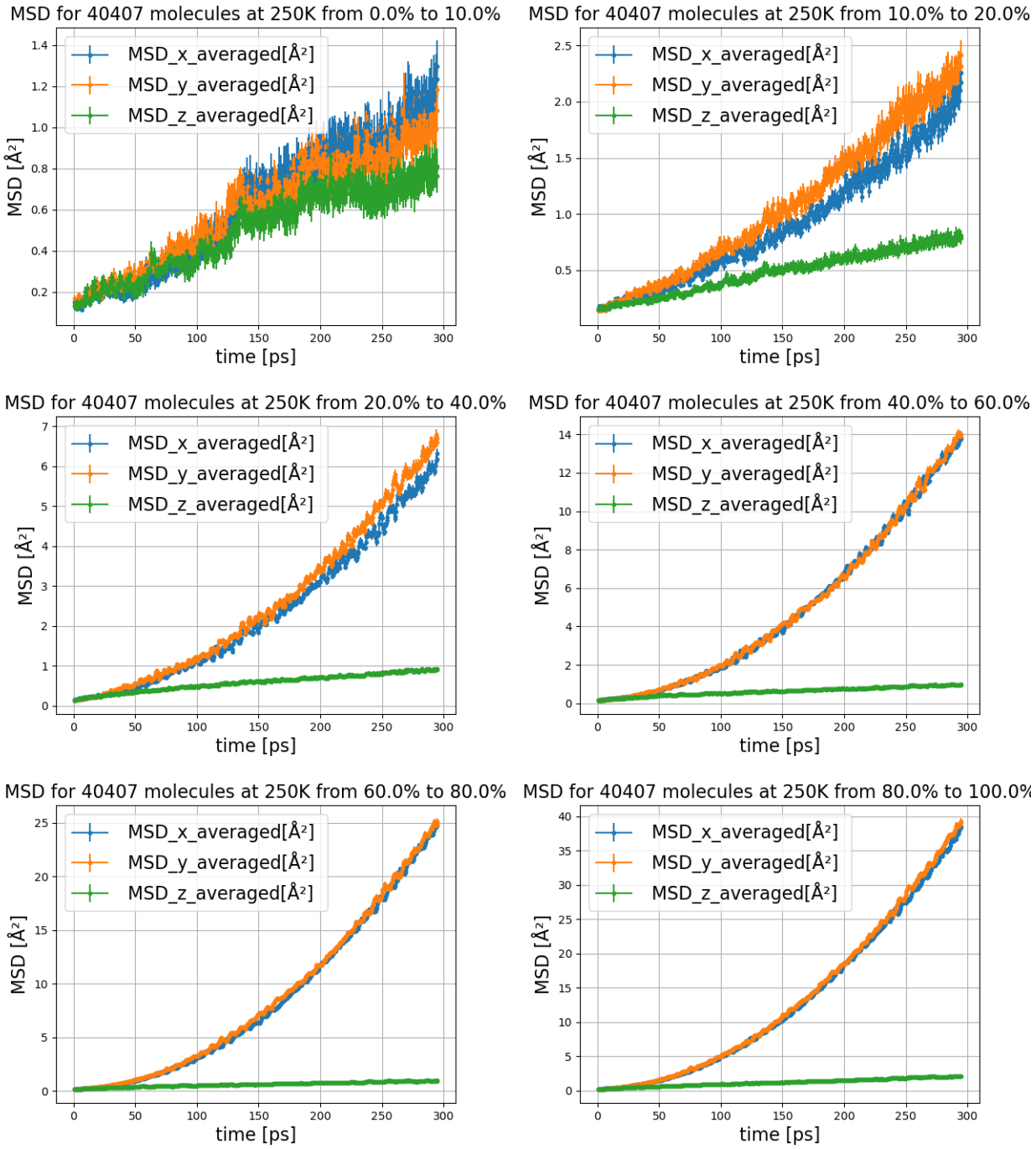

Figure 5.10: MSD for NVT ensemble in cylinder radius of about $69.2\mathring{A}$ with 40407 molecules and periodic boundaries in z-direction for $250K$ for different initial positions over a sample time of the last $300ps$ of a runtime of $400ps$.

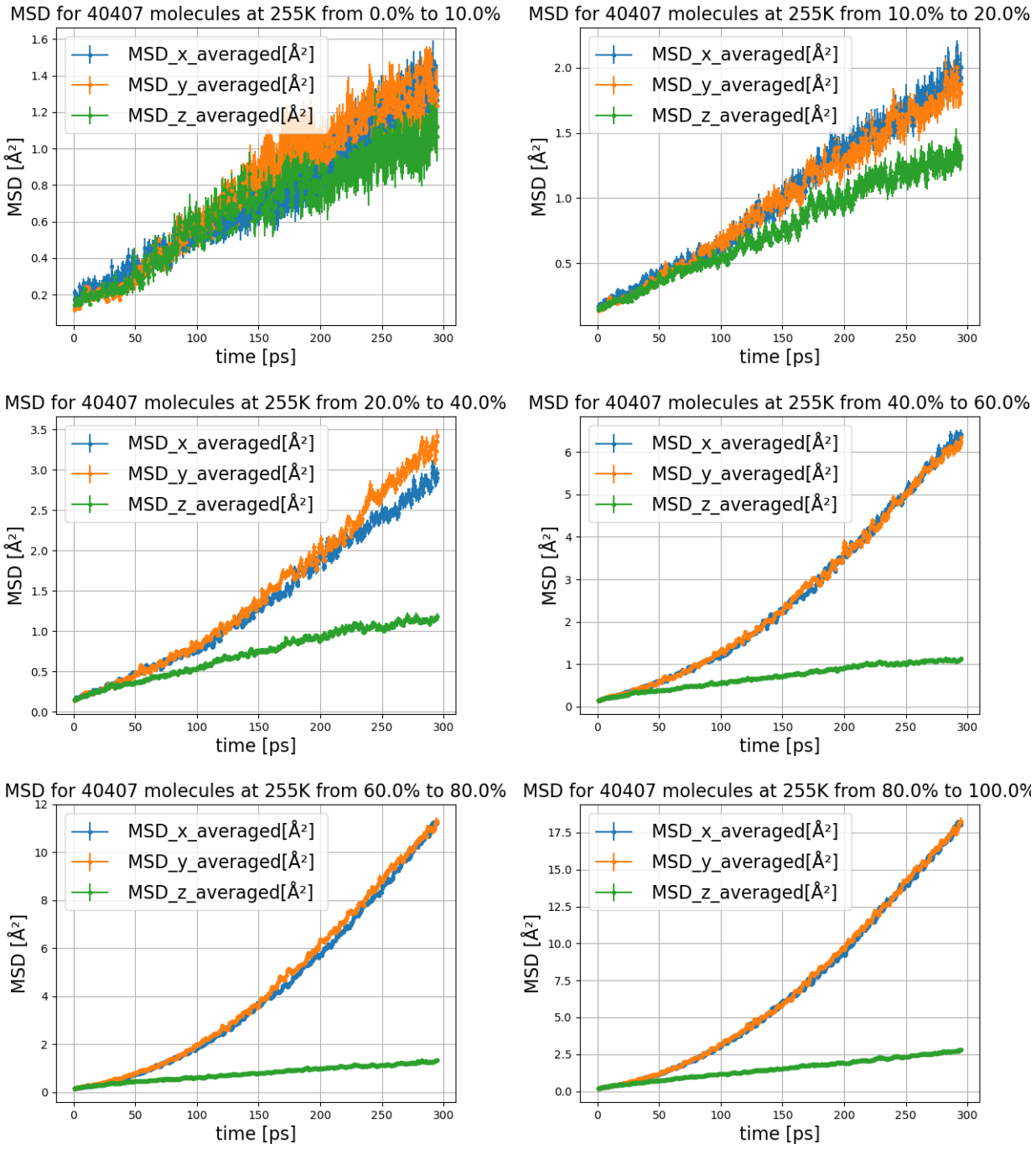

Figure 5.11: MSD for NVT ensemble in cylinder radius of about $69.2\mathring{A}$ with 40407 molecules and periodic boundaries in z-direction for $255K$ for different initial positions over a sample time of the last $300ps$ of a runtime of $400ps$.

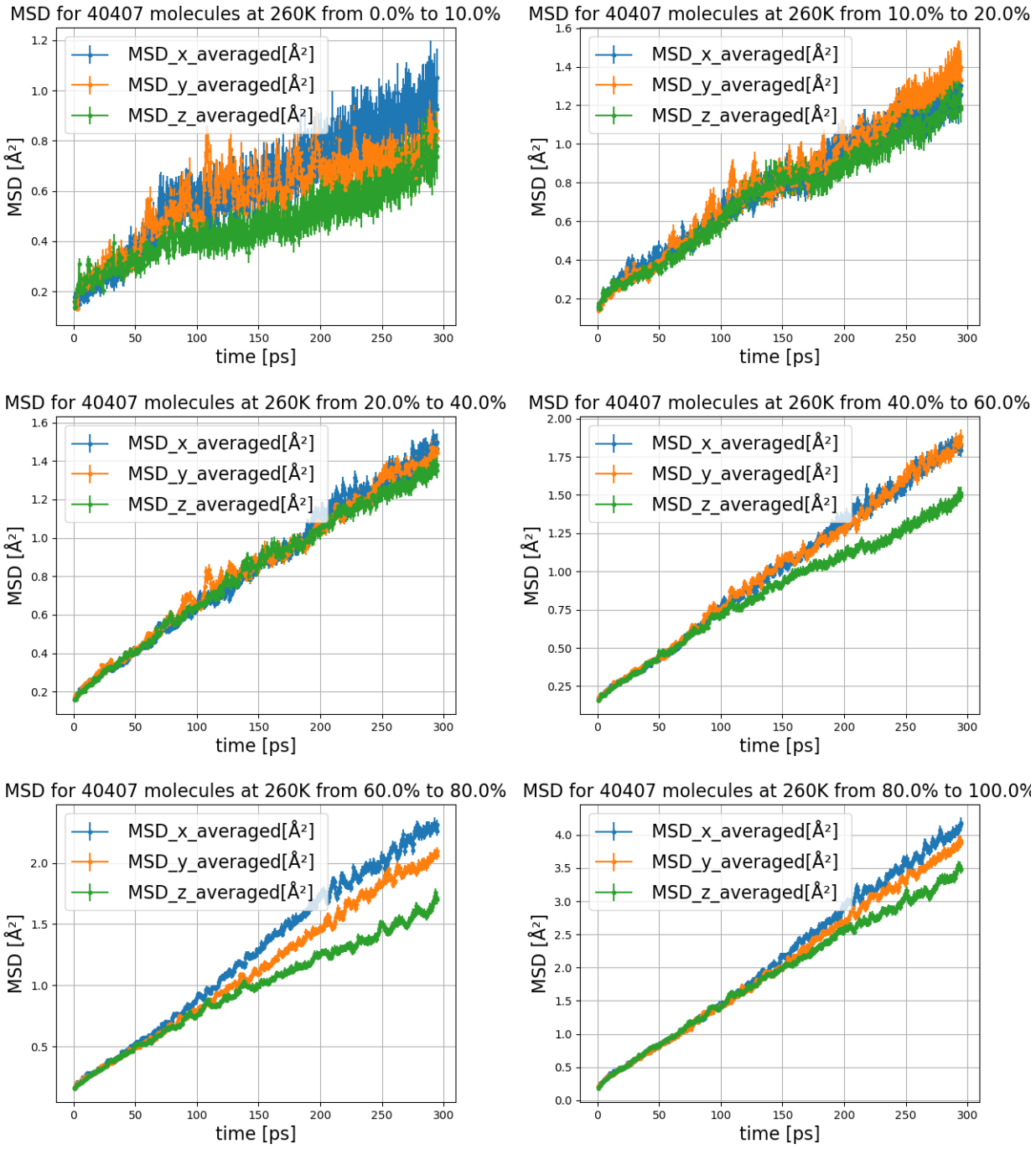

Figure 5.12: MSD for NVT ensemble in cylinder radius of about $69.2\mathring{A}$ with 40407 molecules and periodic boundaries in z-direction for $260K$ for different initial positions over a sample time of the last $300ps$ of a runtime of $400ps$.

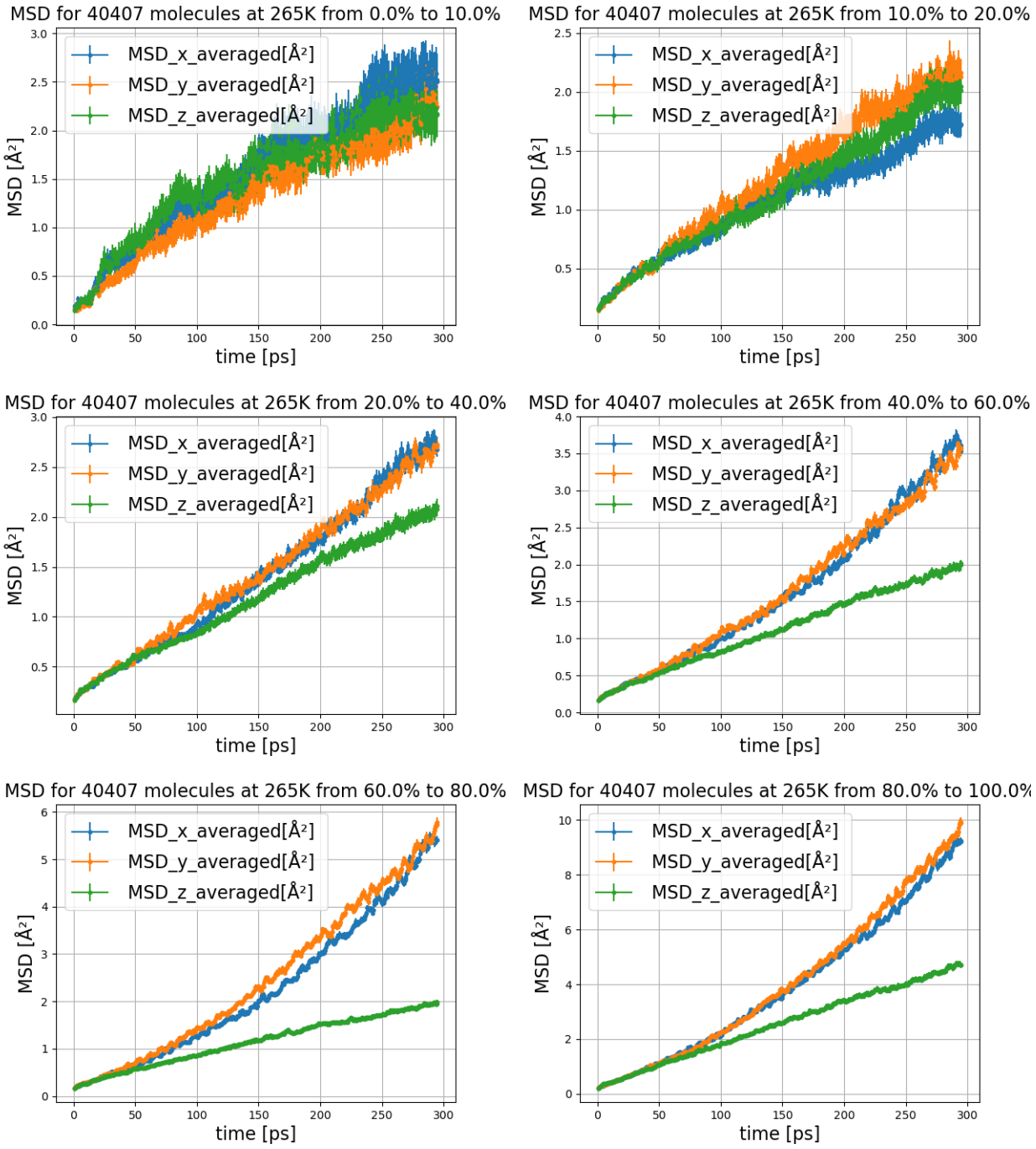

Figure 5.13: MSD for NVT ensemble in cylinder radius of about $69.2\mathring{A}$ with 40407 molecules and periodic boundaries in z-direction for $265K$ for different initial positions over a sample time of the last $300ps$ of a runtime of $400ps$.

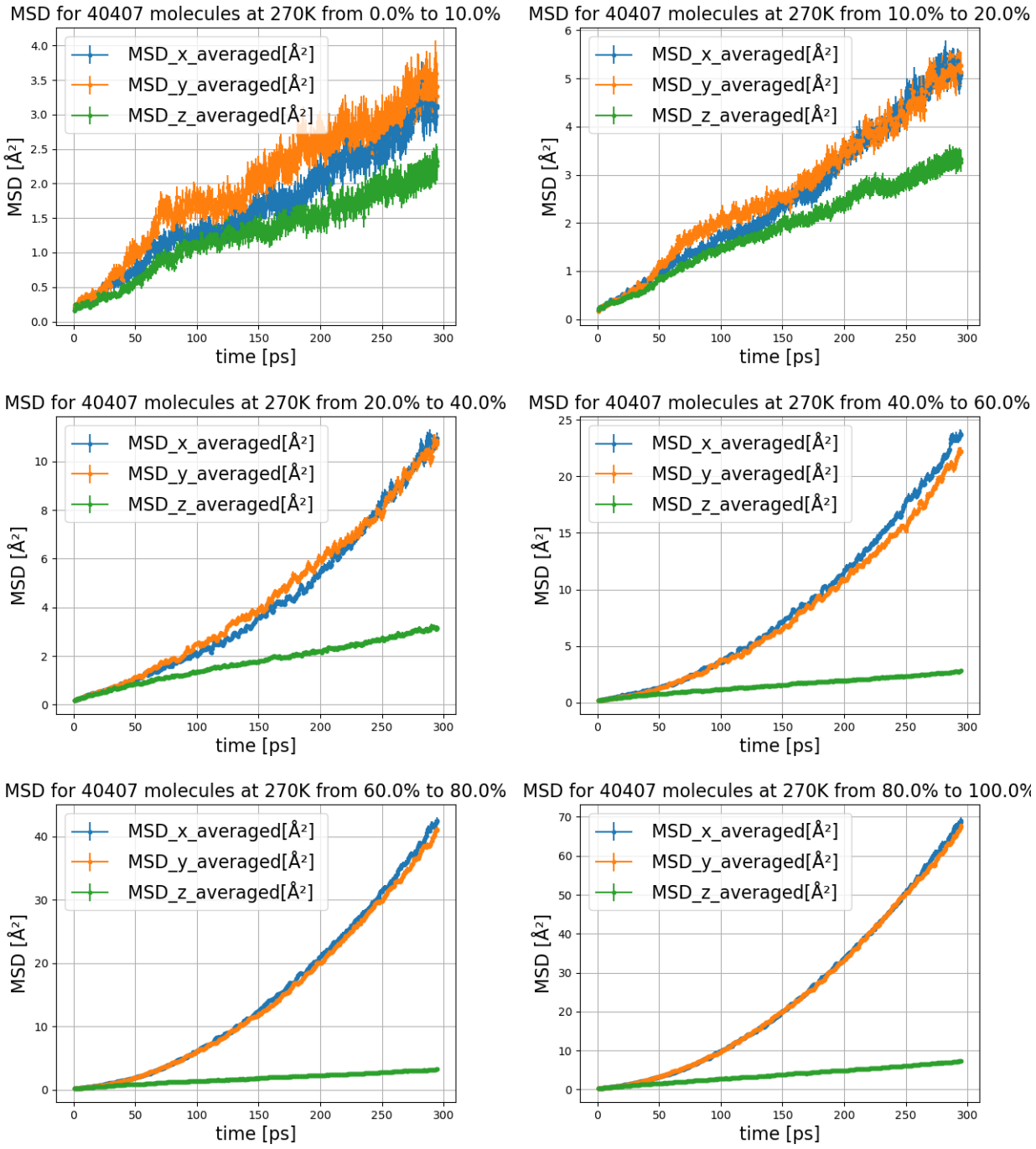

Figure 5.14: MSD for NVT ensemble in cylinder radius of about $69.2\mathring{A}$ with 40407 molecules and periodic boundaries in z-direction for $270K$ for different initial positions over a sample time of the last $300ps$ of a runtime of $400ps$.

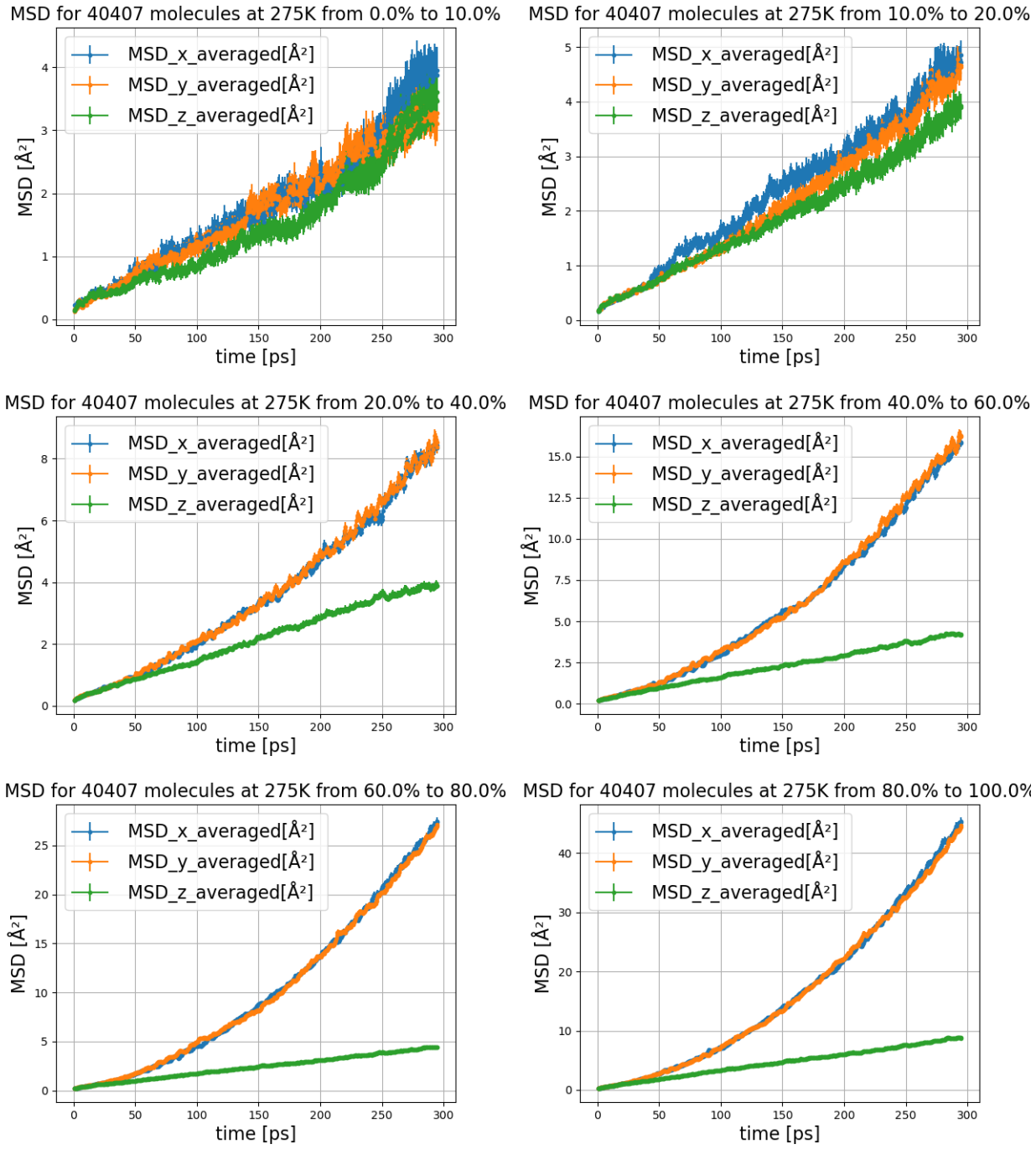

Figure 5.15: MSD for NVT ensemble in cylinder radius of about $69.2\mathring{A}$ with 40407 molecules and periodic boundaries in z-direction for $275K$ for different initial positions over a sample time of the last $300ps$ of a runtime of $400ps$.

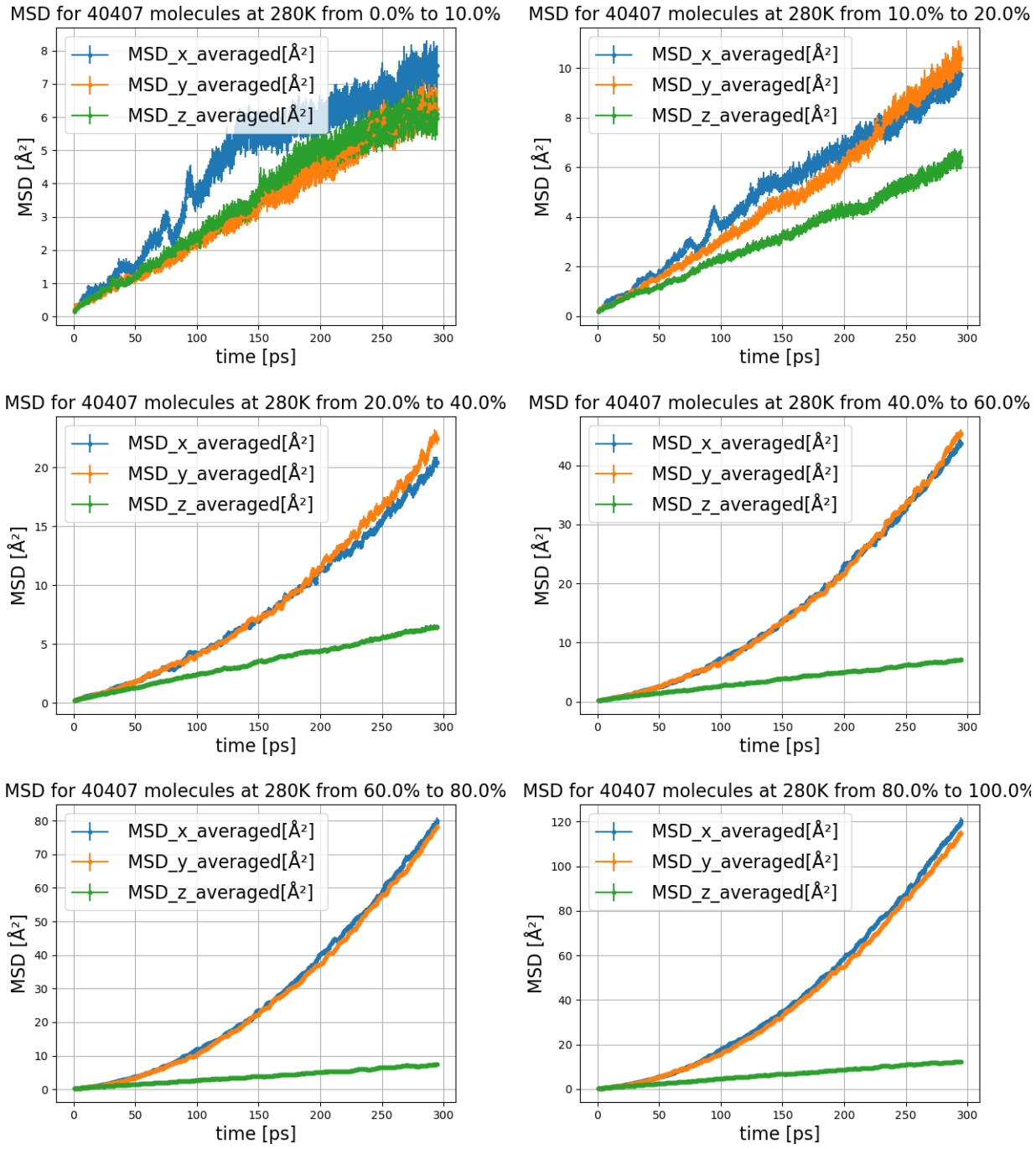

Figure 5.16: MSD for NVT ensemble in cylinder radius of about $69.2\mathring{A}$ with 40407 molecules and periodic boundaries in z-direction for $280K$ for different initial positions over a sample time of the last $300ps$ of a runtime of $400ps$.

We could find no sound arguments to explain the non-linear MSD in figures 4.9 to 4.16 for x- and y-direction. Maybe non-vanishing angular momentum of the ensemble or other effects cause this behaviour.
The MSD for the smaller ensembles had an apparent linear dependency in time for all temperatures, cylinder shells as well as the overall ensembles.

5.4.1 Radius Depending Diffusion Coefficient

In the following figures 4.17 to 4.21 the partial radius corresponds to the relative starting positions. 10 corresponds to molecules initially positioned inside a cylinder shell with 0% to 10% of the wall radius, 20 to a cylinder shell with 10% to 20% of the wall radius and so on. The simulation

for these water (TIP4P/2005) molecules ran for a simulation time of $400ps$. The last $300ps$ were used for the computation of the MSD, from which the diffusion coefficient is derived. The diffusion coefficient was derived by linear interpolation of the ensembles MSD and dividing its slope by 2, as implied by equation 3.10.

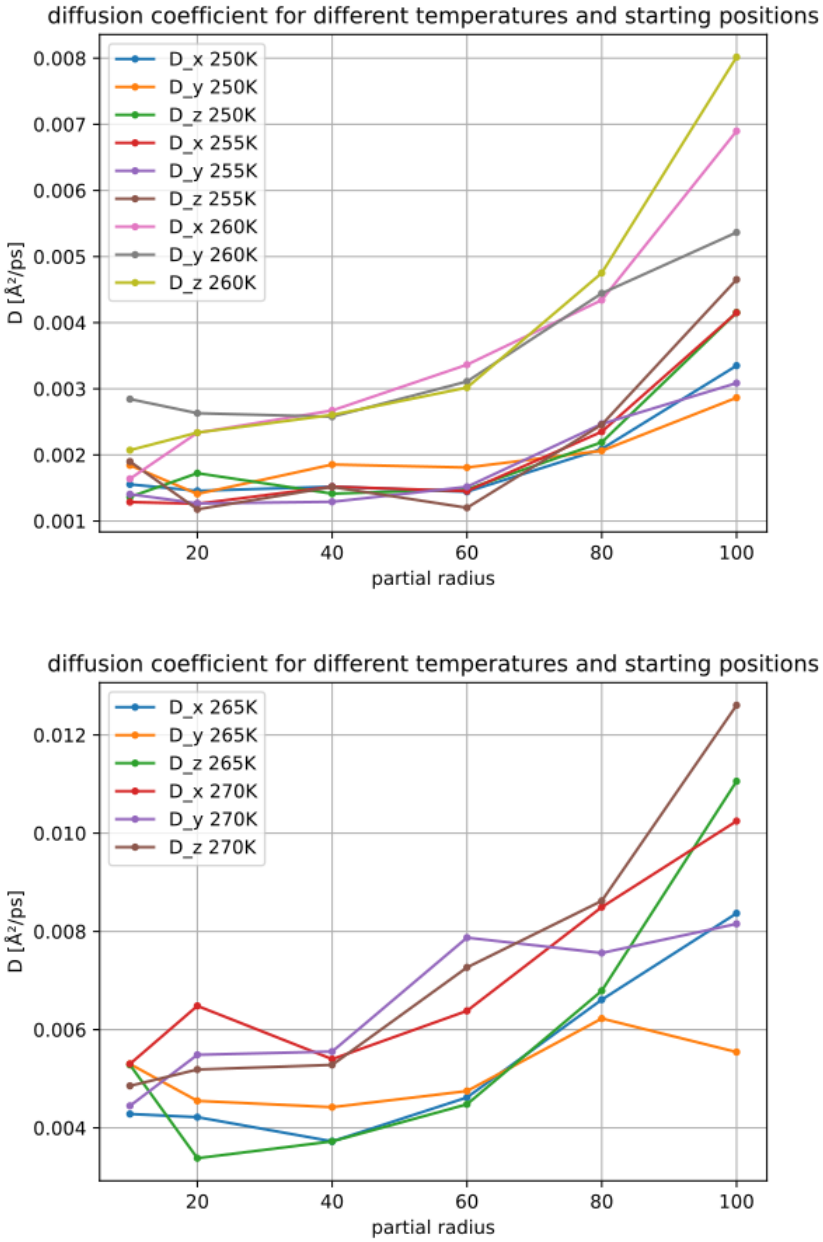

Figure 5.17: Diffusion coefficient for NVT ensemble in cylinder radius of about $28.5\mathring{A}$ with 10427 molecules and periodic boundaries in z-direction for different temperatures.

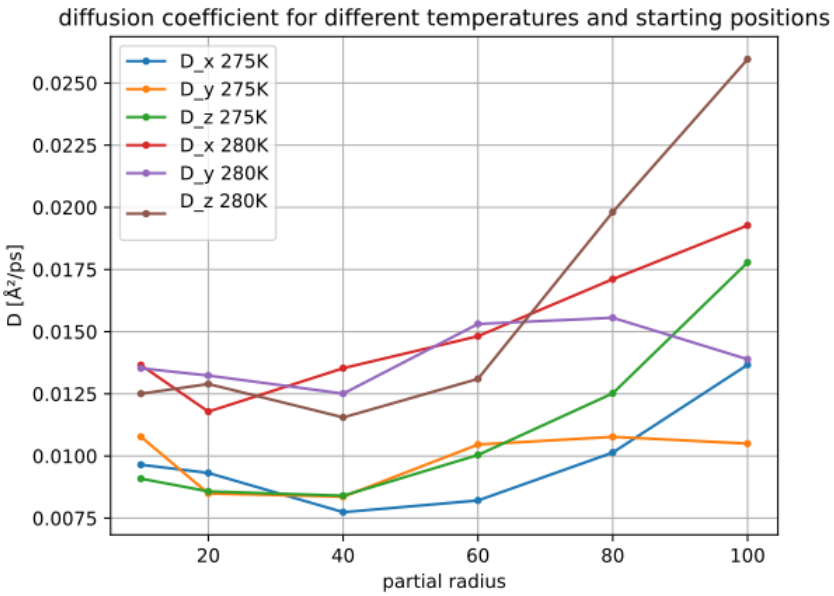

Figure 5.18: Diffusion coefficient for NVT ensemble in cylinder radius of about $28.5\mathring{A}$ with 10427 molecules and periodic boundaries in z-direction for different temperatures.

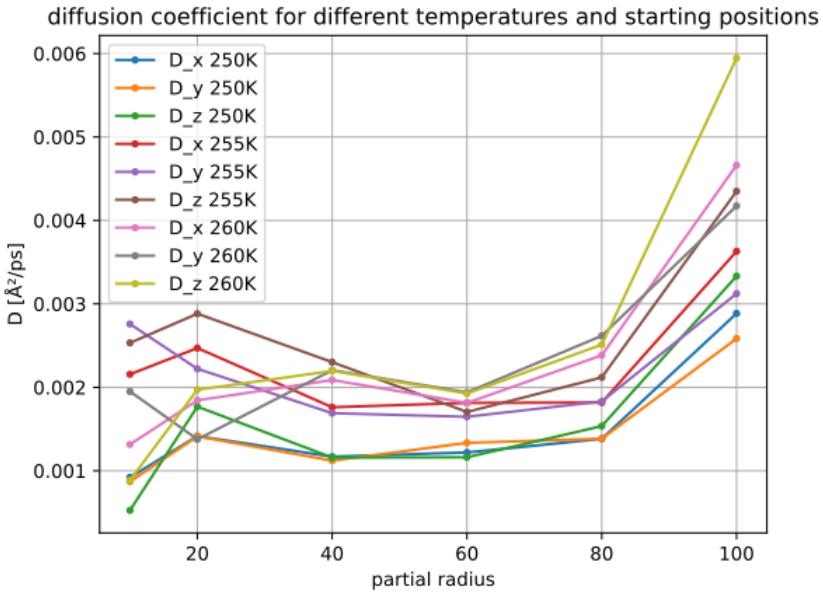

Figure 5.19: Diffusion coefficient for NVT ensemble in cylinder radius of about $41.6\mathring{A}$ with 14075 molecules and periodic boundaries in z-direction for different temperatures.

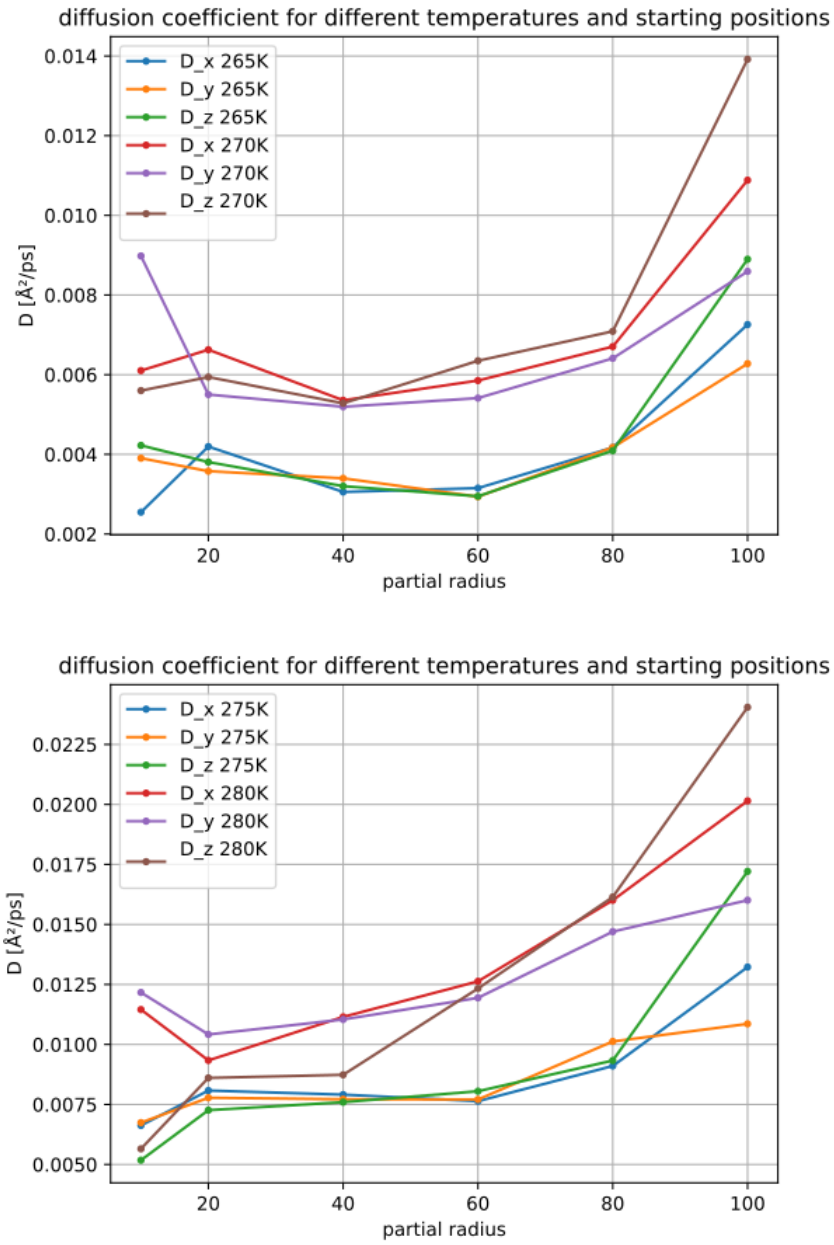

Figure 5.20: Diffusion coefficient for NVT ensemble in cylinder radius of about $41.6\mathring{A}$ with 14075 molecules and periodic boundaries in z-direction for different temperatures.

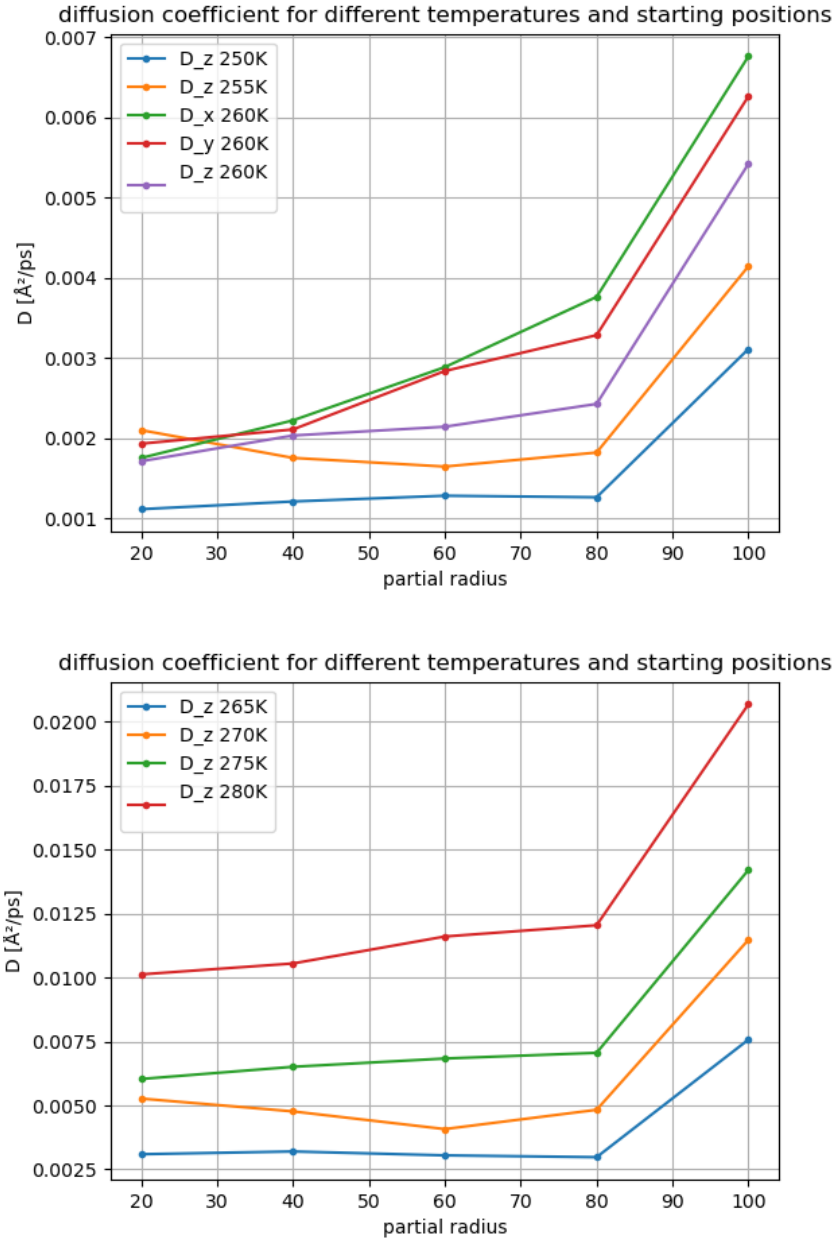

Figure 5.21: Diffusion coefficient for NVT ensemble in cylinder radius of about $69.2\mathring{A}$ with 40407 molecules and periodic boundaries in z-direction for different temperatures. Only data for linear MSD slopes from figures 4.10 to 4.16 were used for these plots.

In figures 4.17 to 4.21 it is clearly visible that molecules initially positioned near the potential wall exert a higher mobility than the ones near the cylinder axis. As expected the wall also diminishes the diffusion in the plane orthogonal to the cylinder axis. This is also clearly discernible from the plots, where the diffusion parallel to the wall of particles initially positioned near the wall is always higher for the ensembles with 10427 molecules and 14075 molecules over all temperatures. The ensembles with 40407 molecules show a different behaviour. In these ensembles the diffusion not only increases for particles initially positioned near the wall. It is also higher for motion in the plane orthogonal to the cylinder axis. When having a look at the overall MSD provided by the LAMMPS log file in figure 4.9 the apparent square growth of the MSD for almost all temperatures (except for $260K$) suggests that the particles either got a lot of free space to move in the plane orthogonal to the cylinder axis, what we would probably see in the density distribution, or another effect causes this behaviour. In figures 4.10 to 4.16 this is also visible not only for the overall ensemble but also for molecules with starting positions in different cylinder shells. Even though the inner two shells, ranging from the cylinder axis up to about 20% of the cylinder radius and for

$260K$ do not show this behaviour at the same scale. It could also be another effect that seems to greatly enable them to move in this plane. Maybe a longer relaxation time in the previous NpT run could reduce this effect. It is also possible that some kind of collective movement causes this non-Brownian motion. To have a look into that possible explanation further investigation would be required.
In summary, it can also be said that we found no clues on the assumption from Schranz et al. that the supercooled water would form a solid core surrounded by liquid water. Especially the density distribution and pair correlation from chapters 4.1 and 4.2 underline this statement.

Bibliography

[1] Water in confined geometries
J. Teixeira et al.
Physica B 234-236 (1997), 370-374
doi: 10.1016/S0921-4526(96)00991-X

[2] Molecular self-diffusion in nanoscale cylindrical pores and classical Fick's law predictions
S. T. Cui
J. Chem. Phys. 123, 054706 (2005)
doi: 10.1063/1.1989314

[3] Dynamic mechanical analysis of supercooled water in nanoporous confinement
Viktor Soprunyuk, Wilfried Schranz, Patrick Huber
EPL 115 46001, 2016
doi: 10.1209/0295-5075/115/46001

[4] https://www.lsbu.ac.uk/about-us/people/people-finder/prof-martin-chaplin#id_first

[5] https://www.chemistryworld.com/features/the-weirdness-of-water/4011260.article

[6] Water: A Tale of Two Liquids
Paola Gallo et al.
Chem. Rev. 2016, 116, 7463-7500
doi: 10.1021/acs.chemrev.5b00750

[7] Structures of High-Density and Low-Density Water
Soper A. K., Ricci M. A.
Phys. Rev. Lett. 2000, 84, 2881-2884
doi: 10.1103/PhysRevLett.84.2881

[8] Water-like anomalies as a function of tetrahedrality
John Russo, Kenji Akahanea and Hajime Tanaka
PNAS, vol. 115, no. 15, E3333–E3341
doi: 10.1073/pnas.1722339115

[9] Perspective on the structure of liquid water
A. Nilsson, L.G.M. Pettersson
https://doi.org/10.1016/j.chemphys.2011.07.021

[10] The structural origin of anomalous properties of liquid water
Anders Nilsson, Lars G.M. Pettersson
doi: 10.1038/ncomms9998 (2015)

[11] Widom line and the liquid–liquid critical point for the TIP4P/2005 water model
José L. F. Abascala and Carlos Vega

The Journal of chemical physics 133, 234502 (2010)
doi: 10.1063/1.3506860

[12] Die zwei Gesichter des Wassers
Rachel Brazil
Spektrum der Wissenschaft, 20.01.2021
https://www.spektrum.de/news/physik-besteht-wasser-aus-zwei-fluessigkeiten/1815494

[13] Glasses and the vitreous state
J. Zarzycki
Chapter 14, p. 361
Cambridge Solid State Science, 1991
ISBN: 0521355826, 9780521355827

[14] http://www.chemistryexplained.com/Ge-Hy/Glass.html

[15] http://www1.lsbu.ac.uk/water/
http://www1.lsbu.ac.uk/water/water_structure_science.html
http://www1.lsbu.ac.uk/water/amorphous_ice.html
http://www1.lsbu.ac.uk/water/water_models.html

[16] Molecular Modeling and Simulation: An Interdisciplinary Guide.
Schlick T.
Interdisciplinary Applied Mathematics series, vol. 21. Springer: New York, NY, USA.
ISBN 0-387-95404-X (2002)
doi: 10.1007/978-1-4419-6351-2_13

[17] http://www.idc-online.com/technical_references/pdfs/chemical_engineering/Water_models.pdf

[18] http://www.sklogwiki.org/SklogWiki/index.php/File:Four_site_water_model.png

[19] https://en.wikipedia.org/wiki/File:Cryst_struct_ice.png

[20] Von Olaf Lenz, Rainald62 - created with Xmgrace by Olaf Lenz, manually modifield by Rainald62, CC BY-SA 3.0
https://commons.wikimedia.org/w/index.php?curid=1820269

[21] Fast Parallel Algorithms for Short-Range Molecular Dynamics
S. Plimpton
J Comp Phys, 117, 1-19 (1995)
https://cs.sandia.gov/~sjplimp/papers/jcompphys95.pdf
https://docs.lammps.org/Intro_overview.html
https://docs.lammps.org/kspace_style.html
https://docs.sandia.gov/
https://docs.lammps.org/Manual.html
https://docs.lammps.org/kspace_modify.html
https://docs.lammps.org/fix_wall.html
https://docs.lammps.org/units.html
https://docs.lammps.org/Howto_tip4p.html

[22] A general purpose model for the condensed phases of water: TIP4P/2005
J. L. F. Abascal, and C. Vega
J. Chem. Phys. 123, 234505 (2005)
https://doi.org/10.1063/1.2121687

[23] Radial distribution functions and densities for the SPC/E, TIP4P and TIP5P models for liquid water and ices I_h, I_c, II, III, IV, V, VI, VII, VIII, IX, XI and XII
Phys. Chem. Chem. Phys., 2005, Volume 7, Issue 7, p 1450-1456
Carlos Vega, Carl McBride, Eduardo Sanza, Jose L. F. Abascala
doi: 10.1039/B418934E

[24] A flexible model for water based on TIP4P/2005
Miguel A. González, and José L. F. Abascal
J. Chem. Phys. 135, 224516 (2011)
https://doi.org/10.1063/1.3663219

[25] https://en.wikipedia.org/wiki/Water_model

[26] Rattle: A "Velocity" Version of the Shake Algorithm for Molecular Dynamics Calculations
Hans C. Andersen, Journal of Computational Physics 52
https://doi.org/10.1016/0021-9991(83)90014-1

[27] Computer Simulation Using Particles
Hockney R. W., Eastwood J. W.
doi: 10.1201/9780367806934

[28] Über die von der molekularkinetischen Theorie der Wärme geforderte Bewegung von in ruhenden Flüssigkeiten suspendierten Teilchen
Albert Einstein
1905, Annalen der Physik, Vol. 4, T. 17
doi: 10.1002/andp.19053220806

[29] Transport coefficients of the TIP4P-2005 water model
Dmitri Rozmanov, Peter G. Kusalik
The Journal of Chemical Physics 136, 044507 (2012)
doi: 10.1063/1.3677196

[30] Transport properties of bulk water at 243 550 K a Comparative molecular dynamics simulation study using SPC E TIP4P and TIP4P 2005 water models
Song Hi Lee and Jahun Kim
MOLECULAR PHYSICS, 2019, VOL. 117, NO. 14, 1926–1933
doi: 10.1080/00268976.2018.1562123

[31] Water diffusion inside carbon nanotubes: mutual effects of surface and confinement
Zheng, Yong-gang and Ye, Hong-fei and Zhang, Zhong-qiang and Zhang, Hong-wu
Phys. Chem. Chem. Phys., 2012, 14, 964–971
doi: 10.1039/C1CP22622C

[32] Diffusion coefficient and shear viscosity of rigid water models
Sami Tazi1 , Alexandru Boţan, Mathieu Salanne , Virginie Marry, Pierre Turq and Benjamin Rotenberg
J. Phys.: Condens. Matter 24 (2012) 284117 (4pp)
doi: 10.1088/0953-8984/24/28/284117

[33] Molecular dynamics study of nanoconfined TIP4P/2005 water: how confinement and temperature affect diffusion and viscosity
A. Zaragoza, M. A. Gonzalez, L. Joly, A. L. Benavidesb, C. Valeriani, I. López-Montero, M. A. Canales
Phys. Chem. Chem. Phys., 2019, 21, 13653
doi: 10.1039/c9cp02485a

[34] System-Size Dependence of Diffusion Coefficients and Viscosities from Molecular Dynamics Simulations with Periodic Boundary Conditions
I.-C. Yeh and G. Hummer
J. Phys. Chem. B 108, 15873 (2004)
doi: 10.1063/1.4960776

[35] Diffusion coefficient and shear viscosity of rigid water models
Sami Tazi, Alexandru Boţan, Mathieu Salanne, Virginie Marry, Pierre Turq, Benjamin Rotenberg
J. Phys.: Condens. Matter 24 (2012) 284117
doi: 10.1088/0953-8984/24/28/284117

[36] System-size corrections for self-diffusion coefficients calculated from molecular dynamics simulations: The case of CO2, n-alkanes, and poly(ethylene glycol) dimethyl ethers
Othonas A. Moultos, Yong Zhang, Ioannis N. Tsimpanogiannis, Ioannis G. Economou, and Edward J. Maginn
The Journal of Chemical Physics 145, 074109 (2016)
doi: 10.1063/1.4960776

[37] https://commons.wikimedia.org/wiki/File:Density_of_ice_and_water_(en).svg

[38] https://en.wikipedia.org/wiki/Radial_distribution_function#/media/File:Rdf_schematic.svg